

WNT signaling in pre-granulosa cells is required for ovarian folliculogenesis and female fertility

Okiko Habara^{1,4}, Catriona Y. Logan², Masami Kanai-Azuma³, Roeland Nusse², Hinako M. Takase^{1,3,4*}

¹Laboratory for Organismal Patterning, RIKEN Center for Biosystems Dynamics Research, Kobe, Japan.

²Howard Hughes Medical Institute, Department of Developmental Biology, Stanford University School of Medicine, Stanford, CA, USA.

³Department of Experimental Animal Model for Human Disease, Center for Experimental Animals, Tokyo Medical and Dental University, Tokyo, Japan.

⁴These authors contributed equally to this research.

*Author for correspondence (hinako.takase@riken.jp)

Keywords

Reproduction, WNT signaling, Folliculogenesis, Oogenesis, Granulosa cells, Oocytes

Summary statement

Canonical WNT signaling is required for postnatal oocyte growth by supporting the activation of surrounding somatic cells in the mouse ovary

Abstract

In mammalian ovaries, immature oocytes are reserved in primordial follicles until their activation for potential ovulation. Precise control of primordial follicle activation (PFA) is essential for reproduction, but how this is achieved is unclear. Here we show that canonical wingless-type MMTV integration site family (WNT) signaling is pivotal for pre-granulosa cell (pre-GC) activation during PFA. We identified several *Wnt* ligands expressed in pre-GCs that act in an autocrine manner. Inhibition of WNT secretion from pre-GCs/GCs by conditional knockout (cKO) of the *Wntless* (*Wls*) gene led to female infertility. In *Wls* cKO mice, GC layer thickness was greatly reduced in growing follicles which resulted in impaired oocyte growth with both an abnormal, sustained nuclear localization of forkhead box O3 (FOXO3) and reduced phosphorylation of ribosomal protein S6 (RPS6). Constitutive stabilization of β -catenin (CTNNB1) in pre-GCs/GCs induced morphological changes of pre-GCs from a squamous into a cuboidal form, though it did not influence oocyte activation. Our results reveal that canonical WNT signaling plays a permissive role in the transition of pre-GCs to GCs, which is an essential step to support oocyte growth.

Introduction

In female mammals, including humans, precise control of folliculogenesis is essential for fertility. Oocytes are protected and grow within follicles, which are the fundamental units of the ovary. Dormant oocytes are arrested at the diplotene stage of meiosis I, reserved in primordial follicles, and surrounded by pre-granulosa cells (pre-GCs) (Pepling, 2006; Pepling and Spradling, 2001). Only a small proportion of primordial follicles is activated concurrently, with activation resulting in follicular growth and the serial development of primary, secondary, preantral, and antral follicles. Although primordial follicles are able to survive for years to decades, once activated their lifespan is limited to days to months, with their potential fates being either ovulation or atresia (McGee and Hsueh, 2000). In women with primary ovarian insufficiency (POI), the number of follicles rapidly declines and menopause occurs before age 40, resulting in severe fertility problems. POI has an estimated prevalence of 1% in women worldwide. The cause of POI remains unknown in most cases, but misregulation of primordial follicle activation (PFA) is regarded as a contributing factor (De Vos et al., 2010; Jankowska, 2017). Therefore, precise control of PFA is required for maintenance of female reproductive ability, as new oocytes are not thought to be generated after birth (Lei and Spradling, 2013).

Given that functional gonadotropin receptors are not present in primordial follicles, PFA is thought to be controlled in a gonadotropin-independent manner (Mason et al., 1986). PFA is characterized morphologically by oocyte growth to a diameter of $>20\text{ }\mu\text{m}$, and proliferation and transition of the squamous pre-GCs into cuboidal/columnar GCs. These two events occur synchronously, indicating that oocyte outgrowth and morphological changes of pre-GCs into GCs are highly coordinated (Adhikari and Liu, 2009). Several intracellular signaling pathways in oocytes have been implicated in control of their dormancy or growth. The transcription factor forkhead box O3 (FOXO3) and the phosphatase and tensin homolog deleted from chromosome 10 (PTEN) are required for the quiescence of oocytes, whereas the phosphoinositide 3-kinase (PI3K)–AKT–mammalian target of rapamycin (mTOR) pathway contributes to oocyte activation (Adhikari et al., 2009; Castrillon et al., 2003; John et al., 2008; Reddy et al., 2008). Additionally, environmental factors such as hypoxia and mechanical stress can influence maintenance of the dormant state of oocytes (Nagamatsu et al., 2019; Shimamoto et al., 2019). In contrast, the

mechanism underlying the activation of pre-GCs is less well understood. Differentiation of pre-GCs was found to be disrupted in mice deficient in *Foxl2* or both GATA binding protein 4 (*Gata4*) and *Gata6*, leading to suppression of the transition from squamous pre-GCs to cuboidal GCs, although gene ablation from the early embryonic period might also affect GC lineage identity (Padua et al., 2014; Schmidt et al., 2004). The transition of pre-GCs to GCs is likely to trigger PFA, given that the associated activation of the mTOR pathway in pre-GCs results in the production of Kit ligand (KITL), which contributes to oocyte activation (Liu et al., 2014). However, a comprehensive understanding of the mechanism of PFA requires clarification of how the transition of pre-GCs to GCs is regulated during this process.

Wingless-type MMTV integration site family (WNT) signaling is an evolutionarily conserved system for cell–cell communication, which is classified broadly into canonical (CTNNB1-dependent, also referred to as WNT/ β -catenin signaling) and noncanonical (CTNNB1-independent) pathways (Martin-Orozco et al., 2019). Nineteen WNT ligands have been identified and contribute to diverse processes such as development, stem cell control, and disease in mice and humans (Nusse and Clevers, 2017; Wiese et al., 2018). Whereas WNT4-mediated canonical WNT signaling has been shown to be important for sex determination during embryonic development (Parma et al., 2006; Vainio et al., 1999), the function of WNT signaling during postnatal folliculogenesis remains unclear. Both *Wnt2* knockout and GC-specific *Wnt4* knockout female mice were found to have slightly reduced fertility, with the mild nature of this defect in each case likely being due to functional redundancy among WNT ligands (Boyer et al., 2010; Monkley et al., 1996). More recently, oocyte-derived R-spondin 2 (RSPO2) was shown to contribute to the activation of WNT signaling in GCs (De Cian et al., 2020). RSPO2 is a WNT agonist that is secreted extracellularly and enhances canonical WNT signaling (Kazanskaya et al., 2004), and follicle growth was found to be impaired in ovaries with loss of RSPO2 function in transplant experiments (De Cian et al., 2020). Although WNT signaling is implicated together with other important factors such as GDF9 (growth differentiation factor 9) and BMP15 (bone morphogenetic protein 15) in PFA (Dong et al., 1996; Dube et al., 1998), its mechanism of action has been unknown. Here we reveal an essential role of canonical WNT signaling in regulation of the transition of pre-GCs to

mature GCs during PFA by focusing on postnatal folliculogenesis and taking advantage of mouse mutants that avoid the issue of the redundancy of WNT ligands.

Results

Canonical WNT signaling in pre-GCs is essential for female fertility. Although WNT signaling has been implicated in adult folliculogenesis, the spatiotemporal patterns of WNT ligand expression in the mouse ovary have been insufficiently characterized (Harwood et al., 2008). Both the complexity and specificity of WNT signaling in mice are due in part to the expression of 19 WNT ligands. To identify the specific WNT ligands that are expressed during folliculogenesis, we performed in situ hybridization analysis with ovaries from 3-week-old wild-type (WT) mice for all 19 *Wnt* mRNAs (Fig. S1). Among the 19 *Wnt* ligands, the mRNAs for *Wnt4*, *Wnt6*, and *Wnt11* were detected in the GC lineage from the primordial follicle to primary follicle stages (Fig. 1A). The abundance of these *Wnt* ligand mRNAs gradually declined in association with the transition to preantral follicles. Minimal expression of *Wnt2*, *Wnt2b*, *Wnt9a*, *Wnt5b*, *Wnt11*, and *Wnt16* was observed in the oocytes of primordial follicles (Figs. 1A, S1). These findings suggest that pre-GC/GC-derived WNT signals might contribute to the early stages of folliculogenesis.

To examine the effects of attenuated WNT signaling, we generated ovarian somatic cell-specific *Wntless* conditional knockout (*Wls* cKO) mice by crossing *Sfl-Cre* mice (which express Cre recombinase under the control of the steroidogenic factor 1 gene (*Nr5a1*) promoter) to mice harboring a “floxed” (*Wls*^{flox}) and a ubiquitous deletion (*Wls*^{del}) allele of *Wls* (Carpenter et al., 2010; Dhillon et al., 2006). Given that WLS is required for secretion of all WNT ligands, the resulting *Sfl-Cre; Wls*^{flox/del} (*Wls* cKO) mice allow us to examine the effects of inhibiting WNT ligand secretion specifically from ovarian somatic cells, including GC and theca lineage cells, from embryonic day (E) 11.5 (Dhillon et al., 2006; Piprek et al., 2019). *Sfl-Cre; Ai9* reporter mouse ovaries were utilized to compute Cre recombination efficiency in FOXL2-positive GC lineage cells, which was 98.30 ± 1.25 % at P0 and 97.37 ± 1.88 % at 2 weeks of age. We found no Cre activity in oocytes. In *Wls* cKO mice, no obvious morphological abnormalities were apparent during development through adulthood (Fig. 1B). To obtain *Wls* cKO mice, female *Wls*^{flox/flox} and male *Sfl-Cre; Wls*^{del/+} mice were mated. The male:female ratio of the resulting

litters was 1.10 (n=500) overall and 1.14 (n=137) for the *Sfl-Cre; Wls^{flox/del}* (*Wls* cKO), with no significant difference by chi-square test. The birth rate of all *Wls* cKO mice was 27.4%, which is close to the theoretical rate of 25.0%. The ovaries of *Wls* cKO mice were similar to those of littermate control mice at postnatal day (P) 0, whereas they manifested atrophy at 2 weeks of age (Fig. 1B). To evaluate reproductive performance, we housed 8-week-old control or *Wls* cKO female mice (*n* = 7 per genotype) with WT males for 24 weeks. *Wls* cKO females were completely infertile (Fig. 1C) even though they engaged in spontaneous mating behavior.

To identify WNT-responding cells, we evaluated the ovaries of a WNT signal reporter mouse line, *R26-WntVis*. The green fluorescent protein (GFP) reporter activity of these mice reflects the activity of the canonical WNT signaling pathway (Takemoto et al., 2016). GFP was specifically expressed in the GC lineage from the primordial to primary follicle stages (Fig. 1D), consistent with the expression pattern of *Wnt* mRNAs (Fig. 1A). FOXL2 was examined as a marker for pre-GCs/GCs and DDX4 as a marker for oocytes in this analysis. The *WntVis* signal was also sparsely detected in the interstitial cells, theca cells, and ovarian epithelium, but not in blood vessels (Fig. S2A–E). It was undetectable in oocytes (Fig. 1D). The *WntVis* signals were most abundant and intense in pre-GCs of primordial follicles, and they became less abundant and less intense with follicle growth (Fig. 1D–F). In the control group, the median was 60.5% for *WntVis*-positive cells in the pre-GC population that were composed of primordial follicles (Fig. 1E). Since primordial follicles contain several pre-GCs, it is expected that most primordial follicles are receiving *Wnt* signaling to some extent. Both the number of *WntVis*-positive pre-GCs/GCs and *WntVis* fluorescence intensity were significantly reduced in *Wls* cKO mice harboring the *R26-WntVis* allele compared to control mice (Fig. 1D–F). Together, these results thus suggested that autocrine WNT signaling activity in pre-GCs is required for female fertility.

WNT signaling is required for the pre-GC to GC transition and subsequent development.

To investigate the cause of the ovarian defects of *Wls* cKO mice, we performed a more detailed morphological analysis (Fig. 2A). Immunostaining of DDX4 revealed that the number of oocytes per ovary did not differ significantly between *Wls* cKO and control mice at P0 (Fig. 2C). Periodic acid–Schiff staining with hematoxylin (PAS-H) revealed few atypical follicles, such as those containing multiple oocytes, in the ovaries of the mutant females at 2 weeks of age (Fig.

2B). Abnormal sexual differentiation was not apparent, as confirmed by sex genotyping (Fig. S3). These data suggested that germ cell survival during embryonic development and sex determination were not affected in *Wls* cKO mice. Whereas cuboidal GCs were apparent in growing follicles containing oocytes with a diameter of 20 to 40 μm in control mice, flattened and morphologically abnormal GCs were detected in *Wls* cKO mice (Fig. 2B). In contrast, no morphological abnormalities were detected in primordial follicles with an oocyte size of $<20 \mu\text{m}$ (Fig. 2B). Quantitative analysis revealed that the GC layer was significantly thinner in growing follicles of *Wls* cKO mice, whereas it was similar in primordial follicles of both genotypes (Fig. 2D,E). GCs in *Wls* cKO mice were less likely to become multilayered, and even when they did form multiple layers, the layers were uneven (Figs. 2B,3A). To describe the morphology of GCs further, we categorized growing follicles by the appearance of GCs as squamous, cuboidal, and columnar (Table S1). Within the growing follicles, primary follicles with squamous GCs were 26.2 % in *Wls* cKO mice, notably higher than the 6.6% observed in controls. Secondary/preantral follicles with columnar GCs with distinct cell polarity were not observed in *Wls* cKO mice, but 48.4% were found in controls. Secondary/preantral follicles in *Wls* cKO mice mainly consisted of cuboidal type cells (27.9%). Overall, these results thus indicated that the PFA-associated transition of pre-GCs to GCs is suppressed in the absence of WNT signaling, yet GCs of some follicles can proceed to the cuboidal stage.

To assess whether WNT signaling might trigger PFA, we quantified the number of follicles per ovary and categorized them by follicle type as primordial (Pm), activated primordial (APF: oocyte diameter of $>20 \mu\text{m}$ without cuboidal GCs), primary (Pr), or secondary–antral (Sec–Ant). at 2 weeks of age. The number of primordial follicles in *Wls* cKO mice was similar to that in control mice (Fig. 2F), suggesting that WNT ligands are not a triggering stimulus but rather a permissive signal for PFA; otherwise, the accumulation of primordial follicles in the mutant ovaries would have been expected. The observation that oocytes larger than 20 μm were present in the ovaries of *Wls* cKO mice (Fig. 2D,E) also suggesting that these cells are capable of initiating a growth response to PFA. However, in contrast to control ovaries, the ovaries of 2-week-old *Wls* cKO mice lacked oocytes with a diameter of 45 to 60 μm . Oocytes with a diameter of $>45 \mu\text{m}$ constituted $26.8 \pm 4.2\%$ (mean \pm s.e.m.) of all oocytes in control females but only $0.5 \pm 0.5\%$ of those in *Wls* cKO females ($P = 0.0286$, nonparametric Mann-Whitney

matched-pairs test) (Fig. 2D). The retardation of oocyte growth in *Wls* cKO mice therefore appeared to occur between PFA and full maturity. The number of developing follicles was significantly lower in *Wls* cKO mice (Fig. 2F), with insufficient GC maturation likely giving rise to follicular atresia.

WNT signaling plays an important role in female sex determination during embryogenesis (Parma et al., 2006; Vainio et al., 1999). We therefore next examined the effects of postnatal deletion of *Wls* with the use of the *Wt1*^{CreERT2} knock-in allele (Zhou et al., 2008). Control and *Wt1*^{CreERT2};*Wls*^{flox/del} (PN-*Wls* cKO) mice were injected with tamoxifen at P3, P5, and P7 to induce *Wls*^{flox} deletion and were studied at 3 weeks of age (Fig. 2G). *Wt1*^{CreERT2};*Ai9* mice showed 99.5 ± 0.18 % efficiency of the Cre recombination within FOXL2-positive cells at 3 weeks of age after tamoxifen administration. The phenotype of PN-*Wls* cKO female mice appeared essentially identical to that of *Wls* cKO females. The PN-*Wls* cKO mice thus showed morphologically normal primordial follicles and attenuated transition of pre-GCs to GCs in growing follicles (Fig. 2H,I). Primary follicles with squamous GCs were 35.6% in PN-*Wls* cKO mice, compared to only 2.4% in controls at 3 weeks of age (Table S2). Hence, the defect found in the pre-GCs to GC transition of *Wls* cKO and PN-*Wls* cKO mice is not the result of disrupted cell fate determination during embryogenesis, but rather a result from the lack of WNT signaling during folliculogenesis. The number of primordial follicles in PN-*Wls* cKO mice was also similar to that of control mice (Fig. 2J), providing further evidence that initiation of PFA can take place without WNT signaling. The ovaries of PN-*Wls* cKO mice also showed reduced numbers of growing follicles (Fig. 2J), reflecting suppression of folliculogenesis.

Functional impairment of the transition of pre-GCs to GCs gives rise to insufficient oocyte activation. To evaluate whether GCs in *Wls* cKO mice are functionally mature, we assessed the expression of anti-Müllerian hormone (AMH), a marker for GCs. Pre-GCs of primordial follicles initially do not express AMH. AMH becomes expressed once GCs grow and transition to a cuboidal/columnar morphology and then is released into the circulation (Visser et al., 2006). In *Wls* cKO mice, however, immunofluorescence staining revealed only a low level of AMH expression in GCs (Fig. 3A). PFA is hypothesized to be a locally regulated process, whereas the later stages of folliculogenesis are influenced markedly by GC-derived paracrine factors and

gonadotropins (Sánchez and Smitz, 2012). We therefore next analyzed major GC-derived hormones (AMH, inhibin A, and estradiol) and gonadotropins (follicle-stimulating hormone (FSH) and luteinizing hormone (LH)) in order to shed light on GC function and the endocrine system in *Wls* cKO mice. The concentrations of AMH and inhibin A in serum were significantly lower in *Wls* cKO female mice than in controls at 8 weeks of age (Fig. 3B,C). These data indicated that GC function is markedly suppressed in *Wls* cKO mice. Estrogens are primarily produced by developing follicles to coordinate systemic reproductive functions (Hillier et al., 1994; Miller and Auchus, 2011), but in this study, their urinary concentration did not differ between the two genotypes (Fig. 3D). Given that estrogen production to some extent has been reported in mutant mice lacking sexual maturation, ovariectomized mice, and human patients whose ovarian steroidogenesis is inhibited (De Tassigny et al., 2007; Miller and Auchus, 2011; Saito et al., 2009), *Wls* cKO mice may also possess a compensatory mechanism that allows for estrogen production. By contrast, the serum levels of FSH and LH were significantly higher in *Wls* cKO mice than in control mice (Fig. 3E,F), possibly reflecting a positive feedback response to the suppressed follicle development and lack of ovulation in the mutant females. Pituitary gland function may thus be normal in *Wls* cKO females, even though *Sfl-Cre* is expressed in endocrine glands (Dhillon et al., 2006). Importantly, low *Amh* and high FSH levels in serum are considered diagnostic criteria for human POI (Jankowska, 2017; Méduri et al., 2007).

GC proliferation is a key contributor to follicle growth, and the mTOR signaling pathway, which is implicated in PFA, appears to regulate GC proliferation (Yu et al., 2011). To assess the role of other signaling pathways such as WNT signaling in GC proliferation, we examined *Wls* cKO mice by performing immunostaining for MKI67 (Ki67) and measuring the signal intensity for all FOXL2-positive GCs within follicles. While the percentage of MKI67-positive GCs increased with follicle growth in both control and *Wls* cKO mice, the increase was less pronounced in the mutant animals (Fig. 3G). Most pre-GCs of primordial follicles were negative for MKI67 in both control and *Wls* cKO mice (Fig. 3G). Transzonal projections (TZPs) are membranous extensions from GCs that pass through the zona pellucida to the oocyte cell membrane and are important for normal oocyte development (Albertini et al., 2001; Carabatsos et al., 1998). Staining of filamentous actin with phalloidin revealed the absence of obvious TZIP structures in *Wls* cKO ovaries (Fig. 3H). These results thus indicated that the abrogated folliculogenesis of *Wls* cKO

mice is attributable to impaired GC proliferation and the inability of GCs to support oocyte growth.

Although we found that oocyte growth is initiated in *Wls* cKO mice, it was unclear whether the oocytes undergo normal activation. To evaluate oocyte status, we analyzed the expression of FOXO3, a transcription factor that contributes to maintenance of oocyte dormancy, by quantifying the nuclear to cytoplasmic ratio of its immunofluorescence intensity (Castrillon et al., 2003). In control mice, whereas primordial follicles manifested a nuclear FOXO3 localization, FOXO3 was exported from the nucleus during PFA (Fig. 3I,J). However, in *Wls* cKO mice, both oocytes with a diameter of <20 μm and those with a diameter of 30 to 40 μm showed a higher FOXO3 intensity in the nucleus than in the cytoplasm (Fig. 3I,J). In both primary and secondary follicles, FOXO3 was localized in the nuclei of growing oocytes of *Wls* cKO mice. FOXO3 is known to be phosphorylated by the PI3K–AKT pathway (John et al., 2008), while phosphorylation of the ribosomal protein S6 (RPS6) is a key downstream event of PI3K–AKT–mTOR pathway in PFA (Adhikari et al., 2009; Reddy et al., 2008). RPS6 contributes to oocyte growth by promoting protein translation and ribosomal biogenesis. Phosphorylated-RPS6 is not obvious in the oocytes of primordial follicles, but once they are activated, it becomes evident. In *Wls* cKO mice, phosphorylated-RPS6 in activated oocytes is markedly suppressed (Fig. 3K,L). This result suggested that the delay in oocyte growth in *Wls* cKO mice (Fig. 2D) is likely due to insufficient function of RPS6. Collectively, these data indicated that, even if oocytes increase in size, they do not undergo the normal activation process in *Wls* cKO mice. These results further suggested that activated GCs are necessary for proper oocyte growth; the functions of FOXO3 and RPS6 via the overlapping PI3K–AKT pathway are under the influence of GCs. We then examined the expression levels of GC-derived KITL and its receptor KIT, which are thought to cause FOXO3 re-localization to the cytoplasm and contribute to oocyte activation (Liu et al., 2014; Saatcioglu et al., 2016). Contrary to our expectations, the expression of KITL and KIT was slightly increased in *Wls* cKO mice (Fig. S4A,B). How loss of WNT signaling might increase KIT and KITL is still a matter that needs further clarification. Nevertheless, the data suggest that in addition to KIT signaling, unknown factors may act downstream of WNT signaling to impact FOXO3 activity.

The pre-GC layer is expanded by a dominant stable form of CTNNB1. To investigate whether WNT signaling is sufficient for the pre-GC transition to GCs, we generated *Wt1*^{CreERT2};*Ctnnb1*^{lox(ex3)/+} (CTNNB1-CA) mice, which express a stable form of CTNNB1 in the somatic lineage of ovaries (Fig. 4A). The stabilized CTNNB1 binds to T cell factor/lymphoid enhancer factor (TCF/LEF) transcription factors, which activate the expression of target genes for canonical WNT signaling (Harada et al., 1999). Ovaries of (tamoxifen-treated) CTNNB1-CA mice were similar in size to those of control mice at 3 weeks of age, but were more spherical in appearance and had a smoother surface compared to control ovaries (Fig. 4B). The observation that somatic cells were densely packed in the ovarian interstitium of CTNNB1-CA mice suggests that hyperproliferation of interstitial cells was responsible for these differences. Morphological abnormalities were not apparent in GCs of growing follicles in the mutant mice, whereas pre-GCs of primordial follicles were not squamous but cuboidal (Fig. 4B). An increase in pre-GC layer thickness was also detected in primordial follicles containing oocytes with a diameter of <20 µm in CTNNB1-CA mice (Fig. 4C), and MKI67 immunostaining revealed that the proliferation of pre-GCs in primordial follicles was enhanced (Fig. 4D). Follicles with oocytes of <20 µm and with four or fewer pre-GCs/GCs that showed no obvious columnar shape were classified as primordial follicles in the mutant ovaries. These results thus revealed that Wnt signaling promotes the transition of pre-GCs to GCs. Of note, CTNNB1-CA mice showed a normal subcellular localization pattern for FOXO3 in their oocytes (Fig. 4E). Given that we believe that WNT plays only a permissive role in PFA, it was not surprising that localization of FOXO3 in oocytes was not affected by hyperactivation of canonical WNT signaling in GCs. However, the expression levels of KITL and KIT were slightly reduced in CTNNB1-CA (Fig. S4C), in contrast to the *Wls* cKO phenotypes. As WNT and KIT signaling are fundamental pathways to regulate the pre-GC transition to GC and oocyte growth, respectively, it is possible that these two pathways can mutually adjust their activity in order to balance the PFA outcome, an idea that can be tested in future studies.

Quantification of follicle number revealed no depletion of primordial follicles or increase in the number of developing follicles in CTNNB1-CA mice (Fig. 4F), suggesting that CTNNB1 stabilization (activation of canonical WNT signaling) is insufficient for induction of PFA. Inhibition of follicle growth was apparent in the mutant mice, however, with the number of

secondary/preantral follicles being significantly reduced (Fig. 4F), and GCs secondary/preantral follicles were less proliferative (Fig. 4D). Constitutive activation of WNT signaling likely influences GCs, interstitial cells, and theca cells in such a manner that the survival and growth of growing follicles are impaired. These characteristics are consistent with the reduced proliferative capacity and cancerous changes of GCs previously observed for mice in which CTNNB1 or the WNT agonist RSPO1 was forcibly expressed (Boerboom et al., 2005; Boerboom et al., 2006; De Cian et al., 2017).

A WNT activator rescues the phenotype of *Wls* cKO mouse ovaries in vitro. To verify the phenotype of *Wls* cKO mice, we determined the effects of a WNT inhibitor in ovarian culture. Ovaries isolated from WT mice at P4 were maintained on membrane cell culture inserts for 6 days by the gas-liquid interphase method, either in the presence of dimethyl sulfoxide (DMSO) as a vehicle control or the WNT inhibitor IWP2, which blocks porcupine O-acyltransferase (PORCN)-mediated palmitoylation and consequent secretion of WNT ligands (Chen et al., 2009) (Fig. 5A). The ovaries at the end of the culture period thus corresponded to ovaries at P10 in vivo. PAS-H staining revealed that IWP2 markedly suppressed GC layer development, whereas it had only a minimal effect on primordial follicles with an oocyte diameter of $<20\ \mu\text{m}$ (Fig. 5B,C). We then cultured ovaries from *Wls* cKO or control mice with the Wnt activator CHIR99021 in an attempt to rescue the phenotype of the mutant ovaries (Fig. 5D). CHIR99021 activates the canonical WNT signaling pathway by inhibiting glycogen synthase kinase 3 (GSK3) and thereby stabilizing CTNNB1 (Bennett et al., 2002). CHIR99021 induced a significant thickening of the GC layer at all assessed follicular stages in both control and *Wls* cKO ovaries (Fig. 5E,F). Of note, the abnormal flattened morphology of GCs in *Wls* cKO ovaries was completely normalized by CHIR99021 treatment (Fig. 5E). These data indicated that the function of WNT signaling in folliculogenesis was evident in vitro, and that a WNT activator was able to promote follicle growth in a commonly adopted culture system.

The mTOR signaling pathway is implicated in PFA. Nutritional or other factors are thus thought to activate mTOR signaling in pre-GCs and thereby stimulate the production of KITL required for oocyte activation (Liu et al., 2014). Given that WNT signaling has been shown to activate mTOR complex 1 (mTORC1) as a result of inhibition of GSK3 (Inoki et al., 2006), we

investigated the potential role of WNT signaling as an upstream regulator of mTOR signaling in GCs. The addition of an activator of mTOR signaling, 3BDO, to ovarian cultures induced a significant increase in GC layer thickness in follicles of *Wls* cKO and control mice (Fig. 5G–I). However, this rescue effect for *Wls* cKO ovaries was limited, even in growing follicles (Fig. 5H,I). These data suggested that WNT and mTOR signaling contribute to PFA in a coordinated manner, rather than through a simple hierarchical relationship.

Discussion

In this study, we propose a postnatal function of canonical WNT signaling to permit the transition of pre-GCs to GCs in an autocrine manner, which is required for facilitating oocyte growth (Fig. 6). Without WNT signaling, the majority of the GC population manifested characteristics similar to pre-GCs, including a squamous shape, hypoproliferative state, limited production of AMH, and lack of TZP formation. WNT-mediated pre-GC to GC transition appears to couple PFA with the nuclear-cytoplasmic shuttling of FOXO3 and phosphorylation of RPS6 in oocytes to exit from dormancy. Since neither attenuation nor enhancement of WNT signaling influences the number of remaining primordial follicles, we hypothesize that the initial trigger for PFA involves other stimuli, but that WNTs are critical regulators of GC activation. Given that *WntVis* signals were undetectable in oocytes, our data do not support the possibility that oocytes directly respond to WNT ligands produced in GCs by activating the canonical WNT signaling pathway, although further studies will be required to fully exclude this possibility. Our findings thus highlight the importance of GC–oocyte communication for functional follicle growth and fertility, taking into consideration the fact that oocytes are able to complete maturation and attain their full size only with the support of GCs whose activation is dependent on WNT signaling.

Our results reveal that WNT signal activation occurs exclusively at the primordial follicle stage. WNT signaling in cuboidal/columnar GCs is likely detrimental to folliculogenesis, given that forced activation of canonical WNT signaling in pre-GCs/GCs reduced the number of developing follicles. Our data are consistent with the previous finding that activation of WNT signaling induced abnormal follicle growth with increased GC apoptosis in an in vitro culture of secondary follicles (Li et al., 2014). The activation of WNT signaling specifically at the

primordial follicle stage is likely achieved as a result of the characteristic expression pattern of *Wnt4/6/11*, which is strongly expressed in the primordial to primary follicle stage, followed by a weaker expression in GCs of preantral follicles as they grow. Because WNT signaling activation occurs during a narrower time window than when the *Wnt* ligands are expressed, additional mechanism may regulate the timing of WNT signaling activation. For example, production of functional RSPO2 by oocytes is important for the activation of canonical WNT signaling in GCs (De Cian et al., 2020). Given that *Rspo2* mRNA was found to be abundant in oocytes of growing follicles, a mechanism likely exists to inhibit WNT signaling after the primary follicle stage. BMP15 has been identified as an inhibitor of WNT signaling during early embryogenesis in *Xenopus* (Di Pasquale and Brivanlou, 2009), and activated mouse oocytes begin to secrete BMP15 at the primary follicle stage (Dube et al., 1998), which makes BMP15 a candidate mediator of WNT signaling in growing follicles. WNT signaling in pre-GCs/GCs may thus be precisely controlled at several levels, including the spatiotemporal specificity of *Wnt* ligand expression and the production of RSPO2 and BMP15 by oocytes.

It was reported that WNT4/RSPO1 initiates ovarian differentiation by activating the canonical WNT signaling pathway at the embryonic stage (Chassot et al., 2014). *Wnt4* is expressed in the gonads of both sexes until E11.5; then, it is repressed in the male gonads and becomes ovary-specific from E12.5 onward. Although partial gonadal sex reversal has been reported in *Wnt4* and *Rspo1* null mice (Parma et al., 2006; Vainio et al., 1999), no such phenotype was observed in the *Wls* cKO mice used in this study. It is possible that the suppression of WNT secretion may have occurred later than gonadal sex determination, since there is likely a delay between the initial expression of Cre recombinase, the deletion of the target *Wls* gene, and the suppression of WNT protein secretion. Since NR5A1 (SF1) expression in somatic cells of female gonads is known to be attenuated after E12.5 (Ikeda et al., 1994), *Wls* cKO under *Sfl*-Cre control may have progressed gradually until birth. It should be noted that the Cre expression starts from E11.5 in the *Sfl*-Cre line we used (Dhillon et al., 2006; Piprek et al., 2019), whereas another *Sfl*-Cre, which is often used in studies of sex differentiation, is reported to be expressed from E10.5 onward (Bingham et al., 2006). Recently Cheng et al. reported GC-specific conditional deletion of *Wls* by utilizing *Amhr2*-Cre that initiates Cre expression from E13.5 (Cheng et al., 2020). They reported impaired luteinization of *Amhr2*-Cre; *Wls*^{flox/flox} mice, while no

abnormalities in sex determination were noticed, which is consistent with the present study. It is possible that Cre-mediated recombination of the *Wls* gene may not be highly efficient, which might explain the absence of sex reversal and the phenotypic difference between *Amhr2-Cre; Wls^{flox/flox}* (homozygous for flox) and *Sf1-Cre; Wls^{flox/del}* (heterozygous for flox and null). We successfully showed the role of postnatal WNT signaling by generating PN-*Wls* cKO mice, but the fetal phenotype of *Wls* cKO ovaries needs to be scrutinized further. Since *Sf1-Cre* is expressed in theca cell lineage as well as pre-GC/GCs, potential role of theca cell-derived WNTs on pre-GC development and PFA should be addressed in follow-up studies utilizing theca cell-specific Cre mice.

Recent progress in the field of in vitro gametogenesis (IVG) has had a great impact on reproductive biology and medicine (Hikabe et al., 2016). Fully developed oocytes can now be obtained from embryonic stem cells or induced pluripotent stem cells of mice by the application of IVG techniques. While the protocol for stem cell-derived oocytes for fertility treatment in humans has not yet been fully established, vigorous research is underway (Yamashiro et al., 2018). Simultaneously, in vitro activation (IVA) has recently been described as an innovative method of fertility treatment for women with POI (Kawamura et al., 2013; Suzuki et al., 2015; Zhai et al., 2016). Wnt-related genes have not been identified as genes responsible for POI, but we have now shown that the hormonal environment of *Wls* cKO mice is similar to that of women with POI (De Vos et al., 2010; Jankowska, 2017). This finding suggests that some cases of POI diagnosed as idiopathic may include those attributable to insufficient transition of pre-GCs to GCs. In IVA method, the oocyte-awakening process (PTEN-PI3K-AKT-FOXO3 signaling) is targeted in order to activate the few remaining primordial follicles. This method is applicable not only to POI patients but also to cancer patients whose only option for having children with their own oocytes is to cryopreserve their ovaries. However, it is hoped that this method will be developed further, because of the 7.8% chance of pregnancy yielded by IVA treatment (Kawamura et al., 2013; Suzuki et al., 2015; Zhai et al., 2016), which is comparable to the estimated 5-10% chance of pregnancy in POI patients (Van Kasteren and Schoemaker, 1999). In this study, treatment of ovarian cultures with the WNT activator CHIR99021 increased the thickness of the GC layer in early developing follicles (oocyte size of 20–40 μ m). It is important to note that such scenario was not observed in response to activation of WNT signaling in

CTNNB1-CA mice; however, this difference may be due to a difference in the extent of WNT signaling activation, or to an effect of CHIR99021 on cell survival (Wang et al., 2015). Given that our study demonstrates that a WNT activator induced GC layer thickening and enhanced follicle growth in vitro, transient administration of a WNT activator such as CHIR99021 or WNT proteins on IVA may prove to be clinically beneficial for enhancing pre-GC transition to GC and thereby to lead efficient PFA and successful pregnancy.

Materials and Methods

Animals. *Sfl-Cre* mice (stock no. 012462), *Wls*^{flox} mice (stock no. 012888), *Wtl*^{CreERT2} mice (stock no. 010912), *Ddx4-Cre* mice (stock no. 006954), and *Ai9* mice (stock no. 007909) were obtained from The Jackson Laboratory (Carpenter et al., 2010; Dhillon et al., 2006; Gallardo et al., 2007; Madisen et al., 2010; Zhou et al., 2008). *Wls*^{del} mice, in which the *Wls*^{flox} allele is deleted ubiquitously, were generated by crossing *Wls*^{flox} mice with *Ddx4-Cre* mice. *R26-WntVis* mice (accession no. CDB0303K) were obtained from Laboratory for Animal Resources and Genetic Engineering at the RIKEN Center for Biosystems Dynamics Research, Kobe, Japan (http://www.clst.riken.jp/arg/reporter_mice.html) (Takemoto et al., 2016). *Ctnnb1*^{lox(ex3)} mice were kindly provided by M. M. Taketo (Kyoto University, Japan) (Harada et al., 1999). *Sfl-Cre;Wls*^{flox/+} and *Wls*^{flox/del} mice were used as littermate controls for *Sfl-Cre;Wls*^{flox/del} (*Wls* cKO) mice. Tamoxifen-injected *Wtl*^{CreERT2}; *Wls*^{flox/+} and *Wls*^{flox/del} mice were used as littermate controls for *Wtl*^{CreERT2}; *Wls*^{flox/del} (PN-*Wls* cKO) mice. Tamoxifen-injected *Wtl*^{CreERT2} and *Ctnnb1*^{lox(ex3)/+} mice were used for littermate control for *Wtl*^{CreERT2}; *Ctnnb1*^{lox(ex3)/+} (CTNNB1-CA) mice. Tamoxifen (0.2 mg per 20 g of body weight) was injected intraperitoneally into mice at P3, P5, and P7. All animal experiments were approved by the Institutional Animal Care and Use Committee of RIKEN (approval number: A2017-13-5). All mouse lines studied were maintained on a mixed genetic background.

Fertility test. Eight-week-old control or *Wls* cKO female mice ($n = 7$ for each genotype) were housed continuously with WT (C57BL/6N) males for 24 weeks, and the numbers of pups produced were counted.

In situ hybridization. In situ hybridization was performed with the use of the RNAscope system (Wang et al., 2012). Ovaries from 3-week-old WT mice were fixed in 10% neutral buffered formalin at room temperature for 24 h, dehydrated, and embedded in paraffin. Tissue sections were processed for in situ detection of RNA with the RNAscope 2.5 High Definition (HD)-Red Assay (ACDBio, Hayward, CA). The probes included those for *Dapb* (catalog no. 310043, accession no. EF191515, target region 414–862), *Wnt4* (catalog no. 401101, accession no. NM_009523.2, target region 2147–3150), *Wnt6* (catalog no. 401111, accession no. NM_009526.3, target region 780–2026), *Wnt11* (catalog no. 405021, accession no. NM_009519.2, target region 818–1643), *Polr2a* (catalog no. 312471, NM_009089.2, target region 2802–3678), *Wnt1* (catalog no. 401091, accession no. NM_021279.4, target region 1204–2325), *Wnt2* (catalog no. 313601, accession no. NM_023653.5, target region 857–2086), *Wnt2b* (catalog no. 405031, accession no. NM_009520.3, target region 1307–2441), *Wnt3* (catalog no. 312241, accession no. NM_009521.2, target region 134–1577), *Wnt3a* (catalog no. 405041, accession no. NM_009522.2, target region 667–1634), *Wnt5a* (catalog no. 316791, accession no. NM_009524.3, target region 200–1431), *Wnt5b* (catalog no. 405051, accession no. NM_001271757.1, target region 319–1807), *Wnt7a* (catalog no. 401121, accession no. NM_009527.3, target region 1811–3013), *Wnt7b* (catalog no. 401131, accession no. NM_009528.3, target region 1597–2839), *Wnt8a* (catalog no. 405061, accession no. NM_009290.2, target region 180–1458), *Wnt8b* (catalog no. 405071, accession no. NM_011720.3, target region 2279–3217), *Wnt9a* (catalog no. 405081, accession no. NM_139298.2, target region 1546–2495), *Wnt9b* (catalog no. 405091, accession no. NM_011719.4, target region 706–1637), *Wnt10a* (catalog no. 401061, accession no. NM_009518.2, target region 479–1948), *Wnt10b* (catalog no. 401071, accession no. NM_011718.2, target region 989–2133), and *Wnt16* (catalog no. 401081, accession no. NM_053116.4, target region 453–1635).

Immunostaining and histology. Immunofluorescence staining was performed with ovaries that had been fixed overnight at 4°C with 4% paraformaldehyde in phosphate-buffered saline (PBS). The fixed tissue was dehydrated, embedded in paraffin, and then sectioned at a thickness of 5 µm. The sections were depleted of paraffin and rehydrated according to standard protocols. For antigen retrieval, they were incubated either at 110°C for 15 min with citrate buffer (pH 6.0) or at 90°C for 20 min with HistoVT One (Nacalai Tesque, Kyoto, Japan). After washing with PBS

containing 0.1% Tween 20 (PBST), the sections were incubated for 1 h at room temperature in a blocking buffer, stained overnight at 4°C with primary antibodies, and then exposed for 2 h at room temperature to a 1:500 dilution of secondary antibodies labeled with Alexa Fluor 488, 568, or 647 (A11057, A-21206, A21447, A21463, and A10042, Thermo Fisher Scientific; or 703-545-155, Jackson ImmunoResearch). The primary antibodies included chicken anti-GFP (1:500 dilution; GFP-1010, Aves Labs), rabbit anti-DDX4 (1:500; ab13840; Abcam), mouse anti-DDX4 (1:200; ab27591, Abcam), goat anti-FOXL2 (1:200; ab5096, Abcam), rabbit anti-AMH (1:100; GTX129593, GeneTex), rabbit anti-FOXO3 (1:500; 12829, Cell Signaling), rat anti-MKI67 (1:400; 14-5698-82, eBioscience), rabbit anti-phospho-RPS6 (1:100, 4857, Cell Signaling), goat anti-KIT (1:100, AF1356, R&D Systems), and rabbit anti-KITL (1:40, ab64677, abcam). Antibodies were diluted in blocking buffer or Can Get Signal immunostain solutions (NKB-401, Toyobo, Osaka, Japan). DNA was counterstained with 4',6-diamidino-2-phenylindole (DAPI). Samples were mounted with VECTASHIELD Vibrance Antifade Mounting Medium (H-1700, Vector Laboratories).

For immunofluorescence staining of GFP, CYP17A1, and PECAM1, ovaries were fixed overnight at 4°C with 4% paraformaldehyde in phosphate-buffered saline (PBS). The fixed tissue was immersed in sucrose gradients (10%, 20%, and 30%) in PBS sequentially at 4 °C; then, tissues were embedded in an optimal cutting temperature compound (OCT). Frozen samples were sectioned at 6 µm using CryoStar NX70 (Leica Microsystems). For antigen retrieval, cryosections were incubated at 70°C for 30 min with HistoVT One (Nacalai Tesque). After washing with PBS containing 0.1% Tween 20 (PBST), the sections were incubated in blocking buffer for 1 h at room temperature, stained overnight at 4°C with primary antibodies, and then exposed for 2 h at room temperature to a 1:500 dilution of secondary antibodies labeled with Alexa Fluor 488, 568, or Dylight 650 (A10042 and SA5-10029, Thermo Fisher Scientific; or 703-545-155, Jackson ImmunoResearch). The following primary antibodies were used: chicken anti-GFP (1:500 dilution; GFP-1010, Aves Labs), rabbit anti-CYP17A1 (1:4,000, 14447-1-AP, Proteintech), and rat anti-PECAM1 (1:100, sc-18916, Santa Cruz Biotechnology). These were diluted in Can Get Signal immunostain solutions (Toyobo, Osaka, Japan). DNA was counterstained with DAPI. Samples were then mounted with VECTASHIELD Vibrance Antifade Mounting Medium (Vector Laboratories).

For phalloidin staining, ovaries fixed with 4% paraformaldehyde in PBS were embedded in Tissue-Tek OCT Compound (Sakura Finetek Japan, Tokyo, Japan) and cryosectioned at a thickness of 6 μ m. The sections were washed with PBST, stained with Alexa Fluor 568–conjugated phalloidin (1:100 dilution; A12380, Thermo Fisher Scientific) and DAPI, and then mounted with VECTASHIELD Vibrance Antifade Mounting Medium (Vector Laboratories).

For Cre recombination efficiency measurements, 6 μ m ovarian cryosections of *Sfl-Cre;Ai9* or tamoxifen-injected *Wt1^{CreERT2};Ai9* mice were treated with goat anti-FOXL2 (1:100 dilution; ab5096, Abcam) and subsequently with donkey anti-goat IgG Alexa Fluor 647 (A21447, Thermo Fisher Scientific), and then mounted with VECTASHIELD Vibrance Antifade Mounting Medium (Vector Laboratories).

PAS-H staining was performed according to a standard protocol. In brief, ovaries were fixed in Bouin's solution, embedded in paraffin, and sectioned at a thickness of 5 μ m. The sections were hydrated and treated first with periodic acid solution for 10 min and then with Schiff's reagent for 15 min. Nuclei were counterstained with hematoxylin.

For quantitative analysis of follicle numbers, Bouin's fixed ovarian sections were immunostained for DDX4. Ovaries fixed with Bouin's solution were embedded in paraffin and were serially sectioned at a thickness of 8 μ m. After treatment with EDTA buffer (pH 8.0) at 110°C for 15 min, every fifth section was incubated consecutively with antibodies to DDX4 (1:500 dilution; ab13840, Abcam) and biotinylated secondary antibodies (1:500; BA-1000, Vector Laboratories). Immune complexes were detected with a Streptavidin Biotin Complex Peroxidase Kit (30462-30, Nacalai Tesque) and Peroxidase Stain DAB Kit (25985-50, Nacalai Tesque). Nuclei were counterstained with hematoxylin.

Image analysis. Immunostaining was examined with a BX53 upright microscope (Olympus) or a slide scanner (Axio Scan.Z1, Zeiss). Phalloidin staining was examined with a confocal laser scanning microscope (TCS SP8, Leica Microsystems). In situ hybridization and PAS-H staining were examined with a slide scanner (Axio Scan.Z1, Zeiss). All images taken with Axio Scan.Z1 utilized the tile scan and automated stitching functions.

For measurement of Cre recombination efficiency, ovarian sections of *Sf1-Cre;Ai9* or *Wt1^{CreERT2};Ai9* mice immunostained for FOXL2 were utilized. Littermate *Ai9* mice were used as negative controls. Images were acquired with a slide scanner (Axio Scan.Z1, Zeiss). The presence or absence of tdTomato fluorescence in FOXL2-positive cells was manually identified on randomly selected ovarian sections from three individuals in each group.

For measurement of WntVis or MKI67 signals in pre-GCs/GCs, ovarian sections were subjected to immunofluorescence staining for GFP or MKI67, respectively, as well as for the GC marker FOXL2 and the oocyte marker DDX4. With the use of ImageJ software (NIH), areas positive for both FOXL2 and DAPI were determined as nuclear regions of GCs. The fluorescence intensity of GFP or MKI67 in each region was measured. The lower thresholds for GFP- or MKI67-positive cells were set at the value with 99% accuracy in the negative control samples. More than five ovaries for each genotype as well as more than one section per ovary were analyzed. Results were summarized according to follicle type: primordial, intermediate (containing an oocyte surrounded by a mixed single layer of pre-GCs and GCs), primary, and secondary/preantral. Only follicles with a visible nucleolus in the oocyte were analyzed.

For quantitative analysis of follicle numbers, Bouin's fixed ovarian sections with immunostaining for DDX4 were analyzed. Only follicles with a visible nucleolus in the oocyte were counted. The raw counts of follicle number were multiplied by 5 to account for the unanalyzed sections and to obtain the estimates of follicle number per ovary. The follicles were classified into primordial follicles (containing an oocyte with a diameter of <20 µm and surrounded by flat pre-GCs), activated primordial follicles (containing an oocyte with a diameter of >20 µm but not containing cuboidal GCs), primary follicles (containing an oocyte surrounded

by a single layer of cuboidal GCs), secondary/preantral follicles (containing an oocyte surrounded by two or more layers of GCs), and antral follicles (containing an oocyte surrounded by multilayered GCs with antral cavity). Seven ovaries for each genotype were analyzed.

For quantification of the subcellular localization of FOXO3, images of immunostained ovarian sections for FOXO3 were analyzed with ImageJ software (NIH). The fluorescence intensity of FOXO3 in cytoplasmic and nuclear (DAPI-positive) regions of oocytes was measured together with oocyte diameter. The nuclear to cytoplasmic ratio of FOXO3 intensity was then determined. More than five ovaries for each genotype, and more than one section per ovary, were analyzed.

For the quantification of phospho-RPS6, KIT, or KITL intensities, images of ovarian sections immunostained for phospho-RPS6, KIT, or KITL were analyzed with ImageJ software (NIH) in the oocyte or the GC area. The regions of GC and oocyte were determined manually by utilizing ImageJ. More than four ovaries for each genotype, and a section per ovary, were analyzed.

The thickness of the GC layer was determined as half the difference between the diameters of the follicle, and the oocyte as measured in PAS-H–stained ovarian sections with the use of ImageJ software (NIH). More than four ovaries for each genotype or treatment, and more than one section per ovary, were analyzed.

For detailed morphometric analyses of growing follicles, primary and secondary follicles were categorized by the appearances of GCs on PAS-H stained Bouin's fixed sections as follows: squamous: more than 70% of GCs are squamous. The aspect ratio of GCs is approximately 2.0–4.0. Squamous/cuboidal: a mixture of flattened and cuboidal cells or GCs show the intermediate feature of squamous and cuboidal. Cuboidal: more than 70% of GCs are cuboidal. The cell aspect ratio is approximately 0.8 to 1.2. Cuboidal/columnar: a mixture of cuboidal and columnar cells or GCs show the intermediate feature of cuboidal and columnar cells. Columnar: nuclei are close to one side of the cytoplasm and show apparent cell polarity. The aspect ratio of GCs is approximately 0.6–0.8. Only follicles with a visible nucleolus in the oocyte were counted in randomly selected sections. More than four ovaries for each genotype, and a section per ovary, were analyzed.

Sex genotyping. For genotyping, we used tail or toe (newborn pups only) snips. The genomic region of *Uba1* was amplified by PCR by using Phire Hot Start II DNA Polymerase (Thermo Fisher Scientific). A primer set to detect *Uba1* (5'-TGGTCTGGACCCAAACGCTGTCCACA-3' and 5'-GGCAGCAGCCATCACATAATCCAGATG-3') was used to determine the chromosomal sexes, as described in a previous report (Chuma and Nakatsuji, 2001). The PCR products were separated by 3.0% agarose gel electrophoresis.

Measurement of hormone levels. Mice at random stages of the estrous cycle were anesthetized with isoflurane prior to cardiac puncture for blood collection, and they were then euthanized by cervical dislocation. Collected blood was allowed to clot at room temperature for at least 30 min before centrifugation at $10,000 \times g$ for 5 min for serum extraction. For collection of urine, mice were manually restrained and allowed to urinate on disposable plastic trays. Serum and urine were stored at -80°C until analysis. AMH, inhibin A, and estradiol concentrations were measured with enzyme-linked immunosorbent assays (Rat and Mouse AMH ELISA, AL-113, Ansh Labs; Equine/Canine/Rodent Inhibin A ELISA, AL-161, Ansh Labs; and Mouse/Rat Estradiol ELISA, ES180S-100, Calbiotech). Serum levels of FSH and LH were determined with the Luminex method (Oriental Yeast, Tokyo, Japan).

Ovarian culture. Ovaries from mice at P4 were cultured on Transwell-COL membranes (3.0- μm pore size, Costar) for 6 days by the gas–liquid interphase method (Morohaku, 2019; Morohaku et al., 2016). The basal culture medium comprised α -minimum essential medium supplemented with 10% fetal bovine serum, 1.5-mM 2-*O*- α -D-glucopyranosyl-L-ascorbic acid (Tokyo Chemical Industry), and penicillin (10 U/ml)–streptomycin (10 $\mu\text{g/ml}$) (Sigma-Aldrich). Ovaries were treated with 2 μM IWP2 (Merck Millipore), 5 μM CHIR99021 (Sigma-Aldrich), or 100 μM 3BDO (Sigma-Aldrich), or with the corresponding concentration of DMSO as a vehicle control. Approximately half of the medium in each well was replaced with fresh medium every other day. The ovaries were maintained at 37°C under 5% CO_2 and 95% air.

Statistical analysis. All statistical analysis was performed with GraphPad Prism 8 or 9 software. Tests included the nonparametric Mann-Whitney matched-pairs test, unpaired multiple *t* tests with the Holm-Sidak correction, two-way analysis of variance (ANOVA) with Sidak's post hoc test for multiple comparisons, and a chi-square test for trend for the contingency table. A *P* value of <0.05 was considered statistically significant.

Acknowledgments

We thank M. M. Taketo for providing *Catnb*^{lox(ex3)} mice; H. Suzuki for helpful discussion; S. Chunxiao for technical assistance; T. A. Katoh, T. Kimura, K. Minegishi, and K. Miyamichi for comments on the manuscript; and H. Hamada and T. S. Kitajima for critical reading of the manuscript.

Competing interests

The authors declare no competing or financial interests.

Author Contributions

H.M.T. designed the project. O.H., C.Y.L., and H.M.T. performed experiments and analyses. M.K.-A., R.N., and H.M.T. interpreted the data and wrote the paper, with contributions from all other authors.

Funding

R.N. is an investigator of the Howard Hughes Medical Institute. This work was supported by the Tomizawa Jun-ichi & Keiko Fund of the Molecular Biology Society of Japan for Young Scientists 2017 as well as by Japan Society for the Promotion of Science KAKENHI grants (17K17690 and 19H05249) to H.M.T.

Data availability

This study did not generate datasets or code.

References

- Adhikari, D. and Liu, K.** (2009). Molecular mechanisms underlying the activation of mammalian primordial follicles. *Endocr. Rev.* **30**, 438–464.
- Adhikari, D., Zheng, W., Shen, Y., Gorre, N., Härmäläinen, T., Cooney, A. J., Huhtaniemi, I., Lan, Z. J. and Liu, K.** (2009). Tsc/mTORC1 signaling in oocytes governs the quiescence and activation of primordial follicles. *Hum. Mol. Genet.* **19**, 397–410.
- Albertini, D. F., Combelles, C. M. H., Benecchi, E. and Carabatsos, M. J.** (2001). Cellular basis for paracrine regulation of ovarian follicle development. *Reproduction* **121**, 647–653.
- Bennett, C. N., Ross, S. E., Longo, K. A., Bajnok, L., Hemati, N., Johnson, K. W., Harrison, S. D. and MacDougald, O. A.** (2002). Regulation of Wnt signaling during adipogenesis. *J. Biol. Chem.* **277**, 30998–31004.
- Bingham, N. C., Verma-Kurvari, S., Parada, L. F. and Parker, K. L.** (2006). Development of a steroidogenic factor 1/Cre transgenic mouse line. *Genesis* **44**, 419–424.
- Boerboom, D., Paquet, M., Hsieh, M., Liu, J., Jamin, S. P., Behringer, R. R., Sirois, J., Taketo, M. M. and Richards, J. A. S.** (2005). Misregulated Wnt/ β -catenin signaling to ovarian granulosa cell tumor development. *Cancer Res.* **65**, 9206–9215.
- Boerboom, D., White, L. D., Dalle, S., Courty, J. and Richards, J. A. S.** (2006). Dominant-stable β -catenin expression causes cell fate alterations and Wnt signaling antagonist expression in a murine granulosa cell tumor model. *Cancer Res.* **66**, 1964–1973.
- Boyer, A., Lapointe, É., Zheng, X., Cowan, R. G., Li, H., Quirk, S. M., Demayo, F. J., Richards, J. S. and Boerboom, D.** (2010). WNT4 is required for normal ovarian follicle development and female fertility. *FASEB J.* **24**, 3010–3025.
- Carabatsos, M. J., Elvin, J., Matzuk, M. M. and Albertini, D. F.** (1998). Characterization of oocyte and follicle development in growth differentiation factor-9-deficient mice. *Dev. Biol.* **204**, 373–384.
- Carpenter, A. C., Rao, S., Wells, J. M., Campbell, K. and Lang, R. A.** (2010). Generation of mice with a conditional null allele for Wntless. *genesis* **48**, 554–558.
- Castrillon, D. H., Miao, L., Kollipara, R., Horner, J. W. and DePinho, R. A.** (2003). Suppression of ovarian follicle activation in mice by the transcription factor Foxo3a. *Science* (80-.). **301**, 215–218.

- Chassot, A. A., Gillot, I. and Chaboissier, M. C.** (2014). R-spondin1, WNT4, and the ctnnb1 signaling pathway: Strict control over ovarian differentiation. *Reproduction* **148**,.
- Chen, B., Dodge, M. E., Tang, W., Lu, J., Ma, Z., Fan, C. W., Wei, S., Hao, W., Kilgore, J., Williams, N. S., et al.** (2009). Small molecule-mediated disruption of Wnt-dependent signaling in tissue regeneration and cancer. *Nat. Chem. Biol.* **5**, 100–107.
- Cheng, J., Li, Y., Zhang, Y., Wang, X., Sun, F. and Liu, Y.** (2020). Conditional deletion of *Wntless* in granulosa cells causes impaired corpora lutea formation and subfertility. *Aging (Albany, NY)*. **12**,.
- Chuma, S. and Nakatsuji, N.** (2001). Autonomous transition into meiosis of mouse fetal germ cells in vitro and its inhibition by gp130-mediated signaling. *Dev. Biol.* **229**, 468–479.
- De Cian, M. C., Pauper, E., Bandiera, R., Vidal, V. P. I., Sacco, S., Gregoire, E. P., Chassot, A. A., Panzolini, C., Wilhelm, D., Pailhous, E., et al.** (2017). Amplification of R-spondin1 signaling induces granulosa cell fate defects and cancers in mouse adult ovary. *Oncogene* **36**, 208–218.
- De Cian, M. C., Gregoire, E. P., Le Rolle, M., Lachambre, S., Mondin, M., Bell, S., Guigon, C. J., Chassot, A. A. and Chaboissier, M. C.** (2020). R-spondin2 signaling is required for oocyte-driven intercellular communication and follicular growth. *Cell Death Differ.* 1–16.
- De Tassigny, X. D. A., Fagg, L. A., Dixon, J. P. C., Day, K., Leitch, H. G., Hendrick, A. G., Zahn, D., Franceschini, I., Caraty, A., Carlton, M. B. L., et al.** (2007). Hypogonadotropic hypogonadism in mice lacking a functional *Kiss1* gene. *Proc. Natl. Acad. Sci. U. S. A.* **104**, 10714–10719.
- De Vos, M., Devroey, P. and Fauser, B. C.** (2010). Primary ovarian insufficiency. *Lancet* **376**, 911–921.
- Dhillon, H., Zigman, J. M., Ye, C., Lee, C. E., McGovern, R. A., Tang, V., Kenny, C. D., Christiansen, L. M., White, R. D., Edelstein, E. A., et al.** (2006). Leptin directly activates SF1 neurons in the VMH, and this action by leptin is required for normal body-weight homeostasis. *Neuron* **49**, 191–203.
- Di Pasquale, E. and Brivanlou, A. H.** (2009). Bone morphogenetic protein 15 (BMP15) acts as a BMP and Wnt inhibitor during early embryogenesis. *J. Biol. Chem.* **284**, 26127–26135.

- Dong, J., Albertini, D. F., Nishimori, K., Kumar, T. R., Lu, N. and Matzuk, M. M.** (1996). Growth differentiation factor-9 is required during early ovarian folliculogenesis. *Nature* **383**, 531–535.
- Dube, J. L., Wang, P., Elvin, J., Lyons, K. M., Celeste, A. J. and Matzuk, M. M.** (1998). The Bone Morphogenetic Protein 15 Gene Is X-Linked and Expressed in Oocytes. *Mol. Endocrinol.* **12**, 1809–1817.
- Gallardo, T., Shirley, L., John, G. B. and Castrillon, D. H.** (2007). Generation of a germ cell-specific mouse transgenic Cre line, Vasa-Cre. *Genesis* **45**, 413–417.
- Harada, N., Tamai, Y., Ishikawa, T. O., Sauer, B., Takaku, K., Oshima, M. and Taketo, M. M.** (1999). Intestinal polyposis in mice with a dominant stable mutation of the β -catenin gene. *EMBO J.* **18**, 5931–5942.
- Harwood, B. N., Cross, S. K., Radford, E. E., Haac, B. E. and De Vries, W. N.** (2008). Members of the WNT signaling pathways are widely expressed in mouse ovaries, oocytes, and cleavage stage embryos. *Dev. Dyn.* **237**, 1099–1111.
- Hikabe, O., Hamazaki, N., Nagamatsu, G., Obata, Y., Hirao, Y., Hamada, N., Shimamoto, S., Imamura, T., Nakashima, K., Saitou, M., et al.** (2016). Reconstitution in vitro of the entire cycle of the mouse female germ line. *Nature* **539**, 299–303.
- Hillier, S. G., Whitelaw, P. F. and Smyth, C. D.** (1994). Follicular oestrogen synthesis: the “two-cell, two-gonadotrophin” model revisited. *Mol. Cell. Endocrinol.* **100**, 51–54.
- Ikeda, Y., Shen, W.-H., Ingraham, H. A. and Parker, K. L.** (1994). *Developmental Expression of Mouse Steroidogenic Factor-1, an Essential Regulator of the Steroid Hydroxylases.*
- Inoki, K., Ouyang, H., Zhu, T., Lindvall, C., Wang, Y., Zhang, X., Yang, Q., Bennett, C., Harada, Y., Stankunas, K., et al.** (2006). TSC2 Integrates Wnt and Energy Signals via a Coordinated Phosphorylation by AMPK and GSK3 to Regulate Cell Growth. *Cell* **126**, 955–968.
- Jankowska, K.** (2017). Premature ovarian failure. *Prz. Menopauzalny* **16**, 51–56.
- John, G. B., Gallardo, T. D., Shirley, L. J. and Castrillon, D. H.** (2008). Foxo3 is a PI3K-dependent molecular switch controlling the initiation of oocyte growth. *Dev. Biol.* **321**, 197–204.

- Kawamura, K., Cheng, Y., Suzuki, N., Deguchi, M., Sato, Y., Takae, S., Ho, C. H., Kawamura, N., Tamura, M., Hashimoto, S., et al.** (2013). Hippo signaling disruption and Akt stimulation of ovarian follicles for infertility treatment. *Proc. Natl. Acad. Sci. U. S. A.* **110**, 17474–17479.
- Kazanskaya, O., Glinka, A., del Barco Barrantes, I., Stannek, P., Niehrs, C. and Wu, W.** (2004). R-Spondin2 is a secreted activator of Wnt/ β -catenin signaling and is required for *Xenopus* myogenesis. *Dev. Cell* **7**, 525–534.
- Lei, L. and Spradling, A. C.** (2013). Female mice lack adult germ-line stem cells but sustain oogenesis using stable primordial follicles. *Proc. Natl. Acad. Sci. U. S. A.* **110**, 8585–8590.
- Li, L., Ji, S. Y., Yang, J. L., Li, X. X., Zhang, J., Zhang, Y., Hu, Z. Y. and Liu, Y. X.** (2014). Wnt/ β -catenin signaling regulates follicular development by modulating the expression of Foxo3a signaling components. *Mol. Cell. Endocrinol.* **382**, 915–925.
- Liu, K., Zhang, H., Risal, S., Gorre, N., Busayavalasa, K., Li, X., Shen, Y., Bosbach, B. and Brännström, M.** (2014). Somatic cells initiate primordial follicle activation and govern the development of dormant oocytes in mice. *Curr. Biol.*
- Madisen, L., Zwingman, T. A., Sunken, S. M., Oh, S. W., Zariwala, H. A., Gu, H., Ng, L. L., Palmiter, R. D., Hawrylycz, M. J., Jones, A. R., et al.** (2010). A robust and high-throughput Cre reporting and characterization system for the whole mouse brain. *Nat. Neurosci.* **13**, 133–140.
- Martin-Orozco, E., Sanchez-Fernandez, A., Ortiz-Parra, I. and Ayala-San Nicolas, M.** (2019). WNT Signaling in Tumors: The Way to Evade Drugs and Immunity. *Front. Immunol.* **10**, 2854.
- Mason, A. J., Hayflick, J. S., Zoeller, R. T., Young, W. S., Phillips, H. S., Nikolics, K. and Seeburg, P. H.** (1986). A deletion truncating the gonadotropin-releasing hormone gene is responsible for hypogonadism in the hpg mouse. *Science* (80-). **234**, 1366–1371.
- McGee, E. A. and Hsueh, A. J. W.** (2000). Initial and cyclic recruitment of ovarian follicles. *Endocr. Rev.* **21**, 200–214.
- Méduri, G., Massin, N., Guibourdenche, J., Bachelot, A., Fiori, O., Kuttann, F., Misrahi, M. and Touraine, P.** (2007). Serum anti-Müllerian hormone expression in women with premature ovarian failure. *Hum. Reprod.* **22**, 117–123.

- Miller, W. L. and Auchus, R. J.** (2011). The molecular biology, biochemistry, and physiology of human steroidogenesis and its disorders. *Endocr. Rev.* **32**, 81–151.
- Monkley, S. J., Delaney, S. J., Pennisi, D. J., Christiansen, J. H. and Wainwright, B. J.** (1996). Targeted disruption of the Wnt2 gene results in placentation defects. *Development* **122**, 3343–3353.
- Morohaku, K.** (2019). A way for in vitro/ex vivo egg production in mammals. *J. Reprod. Dev.* **65**, 281–287.
- Morohaku, K., Tanimoto, R., Sasaki, K., Kawahara-Miki, R., Kono, T., Hayashi, K., Hirao, Y. and Obata, Y.** (2016). Complete in vitro generation of fertile oocytes from mouse primordial germ cells. *Proc. Natl. Acad. Sci. U. S. A.* **113**, 9021–9026.
- Nagamatsu, G., Shimamoto, S., Hamazaki, N., Nishimura, Y. and Hayashi, K.** (2019). Mechanical stress accompanied with nuclear rotation is involved in the dormant state of mouse oocytes. *Sci. Adv.* **5**,.
- Nusse, R. and Clevers, H.** (2017). Wnt/ β -Catenin Signaling, Disease, and Emerging Therapeutic Modalities. *Cell* **169**, 985–999.
- Padua, M. B., Fox, S. C., Jiang, T., Morse, D. A. and Tevosian, S. G.** (2014). Simultaneous gene deletion of Gata4 and Gata6 leads to early disruption of follicular development and germ cell loss in the murine ovary. *Biol. Reprod.* **91**, 24–25.
- Parma, P., Radi, O., Vidal, V., Chaboissier, M. C., Dellambra, E., Valentini, S., Guerra, L., Schedl, A. and Camerino, G.** (2006). R-spondin1 is essential in sex determination, skin differentiation and malignancy. *Nat. Genet.* **38**, 1304–1309.
- Pepling, M. E.** (2006). From primordial germ cell to primordial follicle: Mammalian female germ cell development. *Genesis* **44**, 622–632.
- Pepling, M. E. and Spradling, A. C.** (2001). Mouse ovarian germ cell cysts undergo programmed breakdown to form primordial follicles. *Dev. Biol.* **234**, 339–351.
- Piprek, R. P., Kolasa, M., Podkowa, D., Kloc, M. and Kubiak, J. Z.** (2019). Tissue-specific knockout of E-cadherin (Cdh1) in developing mouse gonads causes germ cells loss. *Reproduction* **158**, 147–157.
- Reddy, P., Liu, L., Adhikari, D., Jagarlamudi, K., Rajareddy, S., Shen, Y., Du, C., Tang, W., Härmäläinen, T., Peng, S. L., et al.** (2008). Oocyte-specific deletion of pten causes premature activation of the primordial follicle pool. *Science* (80-.). **319**, 611–613.

- Saatcioglu, H. D., Cuevas, I. and Castrillon, D. H.** (2016). Control of Oocyte Reawakening by Kit. *PLOS Genet.* **12**, e1006215.
- Saito, T., Ciobotaru, A., Bopassa, J. C., Toro, L., Stefani, E. and Eghbali, M.** (2009). Estrogen contributes to gender differences in mouse ventricular repolarization. *Circ. Res.* **105**, 343–352.
- Sánchez, F. and Smitz, J.** (2012). Molecular control of oogenesis. *Biochim. Biophys. Acta - Mol. Basis Dis.* **1822**, 1896–1912.
- Schmidt, D., Ovitt, C. E., Anlag, K., Fehsenfeld, S., Gredsted, L., Treier, A. C. and Treier, M.** (2004). The murine winged-helix transcription factor Foxl2 is required for granulosa cell differentiation and ovary maintenance. *Development* **131**, 933–942.
- Shimamoto, S., Nishimura, Y., Nagamatsu, G., Hamada, N., Kita, H., Hikabe, O., Hamazaki, N. and Hayashi, K.** (2019). Hypoxia induces the dormant state in oocytes through expression of Foxo3. *Proc. Natl. Acad. Sci. U. S. A.*
- Suzuki, N., Yoshioka, N., Takae, S., Sugishita, Y., Tamura, M., Hashimoto, S., Morimoto, Y. and Kawamura, K.** (2015). Successful fertility preservation following ovarian tissue vitrification in patients with primary ovarian insufficiency. *Hum. Reprod.* **30**, 608–615.
- Takemoto, T., Abe, T., Kiyonari, H., Nakao, K., Furuta, Y., Suzuki, H., Takada, S., Fujimori, T. and Kondoh, H.** (2016). R26-WntVis reporter mice showing graded response to Wnt signal levels. *Genes to Cells.*
- Vainio, S., Heikkilä, M., Kispert, A., Chin, N. and McMahon, A. P.** (1999). Female development in mammals is regulated by Wnt-4 signalling. *Nature* **397**, 405–409.
- Van Kasteren, Y. M. and Schoemaker, J.** (1999). Premature ovarian failure: A systematic review on therapeutic interventions to restore ovarian function and achieve pregnancy. In *Human Reproduction Update*, pp. 483–492.
- Visser, J. A., de Jong, F. H., Laven, J. S. E. and Themmen, A. P. N.** (2006). Anti-Müllerian hormone: A new marker for ovarian function. *Reproduction* **131**, 1–9.
- Wang, F., Flanagan, J., Su, N., Wang, L. C., Bui, S., Nielson, A., Wu, X., Vo, H. T., Ma, X. J. and Luo, Y.** (2012). RNAscope: A novel in situ RNA analysis platform for formalin-fixed, paraffin-embedded tissues. *J. Mol. Diagnostics* **14**, 22–29.

- Wang, X., Wei, L., Cramer, J. M., Leibowitz, B. J., Judge, C., Epperly, M., Greenberger, J., Wang, F., Li, L., Stelzner, M. G., et al.** (2015). Pharmacologically blocking p53-dependent apoptosis protects intestinal stem cells and mice from radiation. *Sci. Rep.* **5**,.
- Wiese, K. E., Nüsse, R. and van Amerongen, R.** (2018). Wnt signalling: Conquering complexity. *Dev.* **145**,.
- Yamashiro, C., Sasaki, K., Yabuta, Y., Kojima, Y., Nakamura, T., Okamoto, I., Yokobayashi, S., Murase, Y., Ishikura, Y., Shirane, K., et al.** (2018). Generation of human oogonia from induced pluripotent stem cells in vitro. *Science* (80-.). **362**, 356–360.
- Yu, J., Yaba, A., Kasiman, C., Thomson, T. and Johnson, J.** (2011). mTOR Controls Ovarian Follicle Growth by Regulating Granulosa Cell Proliferation. *PLoS One* **6**, e21415.
- Zhai, J., Yao, G., Dong, F., Bu, Z., Cheng, Y., Sato, Y., Hu, L., Zhang, Y., Wang, J., Dai, S., et al.** (2016). In Vitro Activation of Follicles and Fresh Tissue Auto-transplantation in Primary Ovarian Insufficiency Patients. *J. Clin. Endocrinol. Metab.* **101**, 4405–4412.
- Zhou, B., Ma, Q., Rajagopal, S., Wu, S. M., Domian, I., Rivera-Feliciano, J., Jiang, D., Von Gise, A., Ikeda, S., Chien, K. R., et al.** (2008). Epicardial progenitors contribute to the cardiomyocyte lineage in the developing heart. *Nature* **454**, 109–113.

Figure Legends

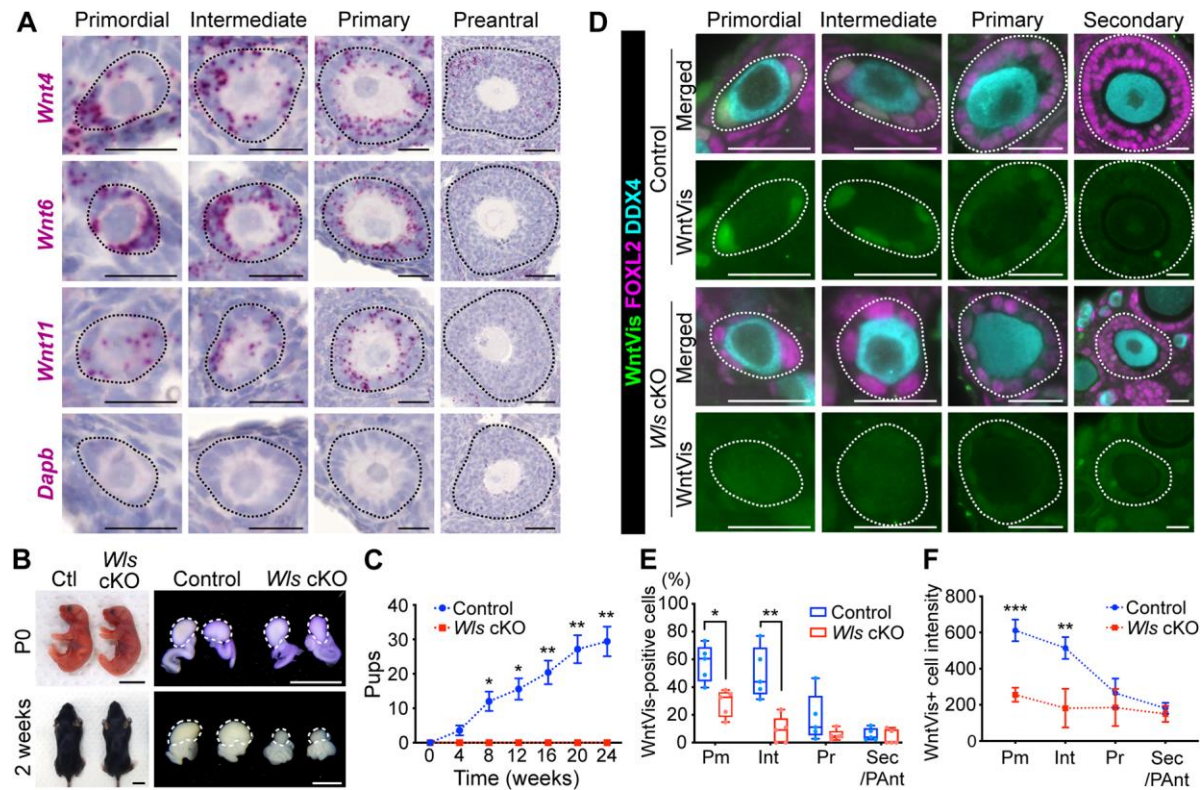


Figure 1. Canonical WNT signaling in primordial follicles. (A) In situ hybridization analysis of *Wnt4*, *Wnt6*, *Wnt11*, and *Dapb* (negative control) mRNAs (red) in ovaries of 3-week-old WT mice. Follicles were classified as primordial, intermediate, primary, or preantral (dotted lines). Scale bar, 50 μ m (rightmost panels) or 20 μ m (other panels). (B) Gross morphology of the body and ovaries (dotted lines) of *Wls* cKO and littermate control (Ctl) mice at P0 and 2 weeks of age. Black scale bar, 1 cm; white scale bar, 100 μ m. (C) Cumulative number of pups born to control or *Wls* cKO female mice housed with WT males for 24 weeks beginning at 8 weeks of age. Data are means \pm s.e.m. ($n=7$ females of each genotype). * $P < 0.05$, ** $P < 0.01$ (two-way ANOVA with Sidak's test for multiple comparisons). (D) Immunofluorescence staining of WntVis (green), FOXL2 (magenta), and DDX4 (cyan) in the ovaries of 3-week-old *Wls* cKO and littermate control mice harboring the *R26-WntVis* allele. White dotted lines indicate follicles. Scale bar, 20 μ m. (E) Percentage of WntVis-positive cells among pre-GCs/GCs for each follicle type (Pm, primordial; Int, intermediate; Pr, primary; Sec/PAnt, secondary/preantral) as determined from images as in (D). Boxes indicate the median and 25th and 75th percentiles, the whiskers indicate

minimum and maximum values ($n=5$ mice of each genotype). $**P < 0.01$, $***P < 0.001$ (unpaired multiple t tests with the Holm-Sidak correction). (F) Fluorescence intensity of WntVis-positive cells for each follicle type. Data are means \pm 95% confidence interval ($n=725$ cells from five control mice; $n=256$ cells from five *Wls* cKO mice). $**P < 0.01$, $***P < 0.001$ (unpaired multiple t tests with the Holm-Sidak correction).

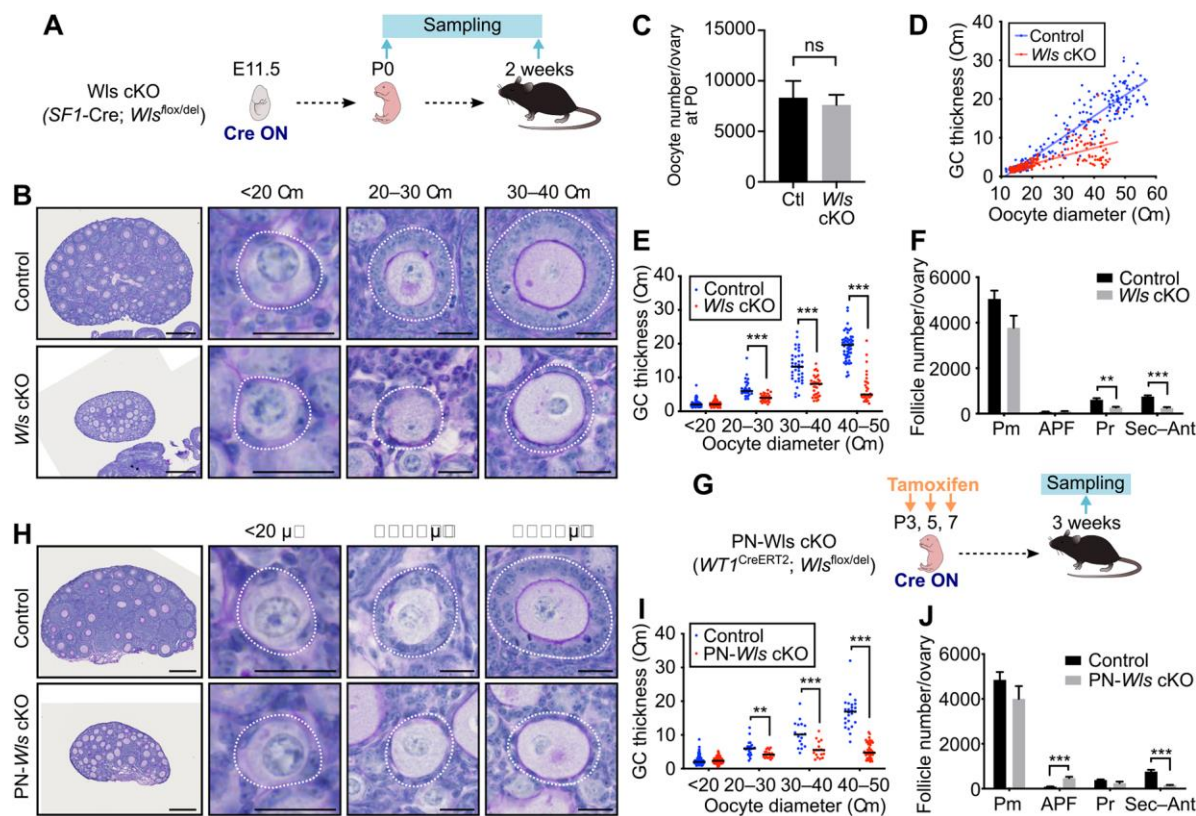


Figure 2. *Wls* cKO mice show an impaired transition of pre-GCs to GCs. (A) Experimental scheme for examination of *Wls* cKO mice to determine the effects of embryonic deletion of *Wls* in ovarian somatic cells on folliculogenesis. (B) PAS-H staining of ovarian sections from 2-week-old *Wls* cKO mice. Follicles were classified by oocyte size (white dotted lines). Scale bar, 200 μm (leftmost panels) or 20 μm (other panels). (C) The number of DDX4-positive oocytes per ovary of *Wls* cKO or littermate control (Ctl) mice, as determined by immunohistochemical staining at P0. Data are means + s.e.m. ($n=7$ mice of each genotype). ns, not significant (nonparametric Mann-Whitney matched-pairs test). (D) Scatter plot for the distribution of oocyte diameter and GC layer thickness for follicles of 2-week-old *Wls* cKO ($n=200$ follicles) and control ($n=236$ follicles) mice as determined from images similar to those in (B). Regression lines are included. (E) GC layer thickness categorized by oocyte diameter for follicles of 2-week-old *Wls* cKO mice ($n=208$ follicles from four control mice; $n=200$ follicles from four *Wls* cKO mice). Horizontal lines represent the median. *** $P < 0.001$ (unpaired multiple t tests with the Holm-Sidak correction). (F) Quantification of follicle number per ovary for 2-week-old *Wls* cKO mice as determined by immunohistochemical staining for DDX4. Follicles were

classified as primordial (Pm), activated primordial (APF: oocyte diameter of $>20\ \mu\text{m}$ without cuboidal GCs), primary (Pr), or secondary–antral (Sec–Ant). Data are means + s.e.m. ($n=7$ mice per genotype). $**P < 0.01$, $***P < 0.001$ (unpaired multiple t tests with the Holm-Sidak correction). (G) Experimental scheme for examination of PN-*Wls* cKO mice to determine the effects of postnatal deletion of *Wls* on folliculogenesis in ovarian somatic cells. (H) PAS-H staining of ovarian sections from tamoxifen-treated 3-week-old PN-*Wls* cKO mice. (I) GC layer thickness categorized by oocyte diameter for follicles of 3-week-old PN-*Wls* cKO mice ($n=239$ follicles from six control mice; $n=315$ follicles from six PN-*Wls* cKO mice). Horizontal lines represent the median. $**P < 0.01$, $***P < 0.001$ (unpaired multiple t tests with the Holm-Sidak correction). (J) Quantification of follicle number per ovary for 3-week-old PN-*Wls* cKO mice as determined by immunohistochemical staining for DDX4. Follicles were classified as primordial (Pm), activated primordial (APF: oocyte diameter of $>20\ \mu\text{m}$ without cuboidal GCs), primary (Pr), or secondary–antral (Sec–Ant). Data are means + s.e.m. ($n=7$ mice per genotype). $***P < 0.001$ (unpaired multiple t tests with the Holm-Sidak correction).

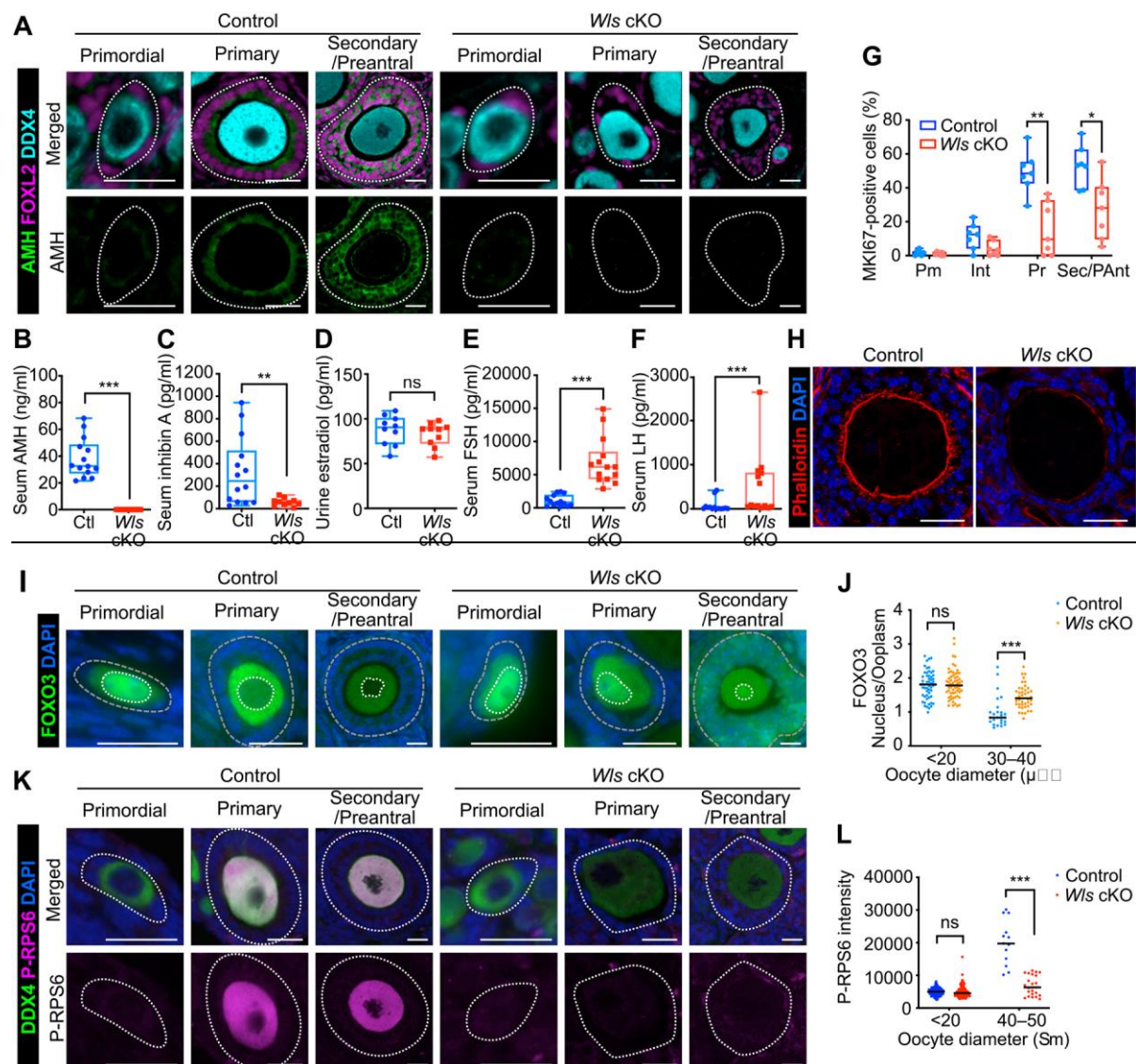


Figure 3. Pre-GC to GC transition and oocyte activation are suppressed in *Wls* cKO mice.

(A) Immunostaining of AMH (green), DDX4 (cyan), and FOXL2 (magenta) in the ovaries of 3-week-old *Wls* cKO or littermate control mice. Follicles are demarcated with white dotted lines. Scale bar, 20 μ m. (B–F) Levels of AMH (B) and inhibin A (C) in serum, of estradiol in urine (D), and of FSH (E) and LH (F) in serum of 8-week-old *Wls* cKO and control (Ctl) mice. ($n=14$ for control and $n=10$ for *Wls* cKO (B, C), $n=10$ (D), $n=14$ (E, F).) The boxes indicate the median and 25th and 75th percentiles, and the whiskers represent minimum and maximum values. ** $P < 0.01$, *** $P < 0.001$; ns, not significant (nonparametric Mann-Whitney matched-pairs test). (G) Percentage of MKI67-positive pre-GCs/GCs for each follicle type (Pm, primordial; Int,

intermediate; Pr, primary; Sec/PAnt, secondary/preantral) in 3-week-old *Wls* cKO and control mice ($n=7$) as determined by immunofluorescence staining. $*P < 0.05$, $**P < 0.01$ (unpaired multiple t tests with the Holm-Sidak correction). (H) Staining of actin fibers with phalloidin (red) and of nuclei with DAPI (blue) for growing follicles from 3-week-old *Wls* cKO or control mice. Scale bar, 25 μm . (I) Immunofluorescence staining of FOXO3 (green) for oocytes of 4-week-old *Wls* cKO or control mice. Nuclei were counterstained with DAPI (blue). White and gray dotted lines mark the boundaries of each oocyte nucleus and follicles, respectively. Scale bar, 20 μm . (J) The nucleus/cytoplasm ratio of FOXO3 fluorescence intensity in oocytes determined from images similar to those in (I). Horizontal lines represent the median ($n=80$ oocytes from four control mice; $n=102$ oocytes from four *Wls* cKO mice). $***P < 0.001$; ns, not significant (unpaired multiple t tests with the Holm-Sidak correction). (K) Immunostaining of phospho-RPS6 (P-RPS6, magenta) and DDX4 (green) in the ovaries of 3-week-old *Wls* cKO or littermate control mice. Nuclei were counterstained with DAPI (blue). Follicles are demarcated with white dotted lines. Scale bar, 20 μm . (L) Fluorescence intensity of P-RPS6 in oocytes determined from images similar to those in (K). Horizontal lines represent the median ($n=136$ oocytes from four control mice; $n=220$ oocytes from five *Wls* cKO mice). $***P < 0.001$; ns, not significant (unpaired multiple t tests with the Holm-Sidak correction).

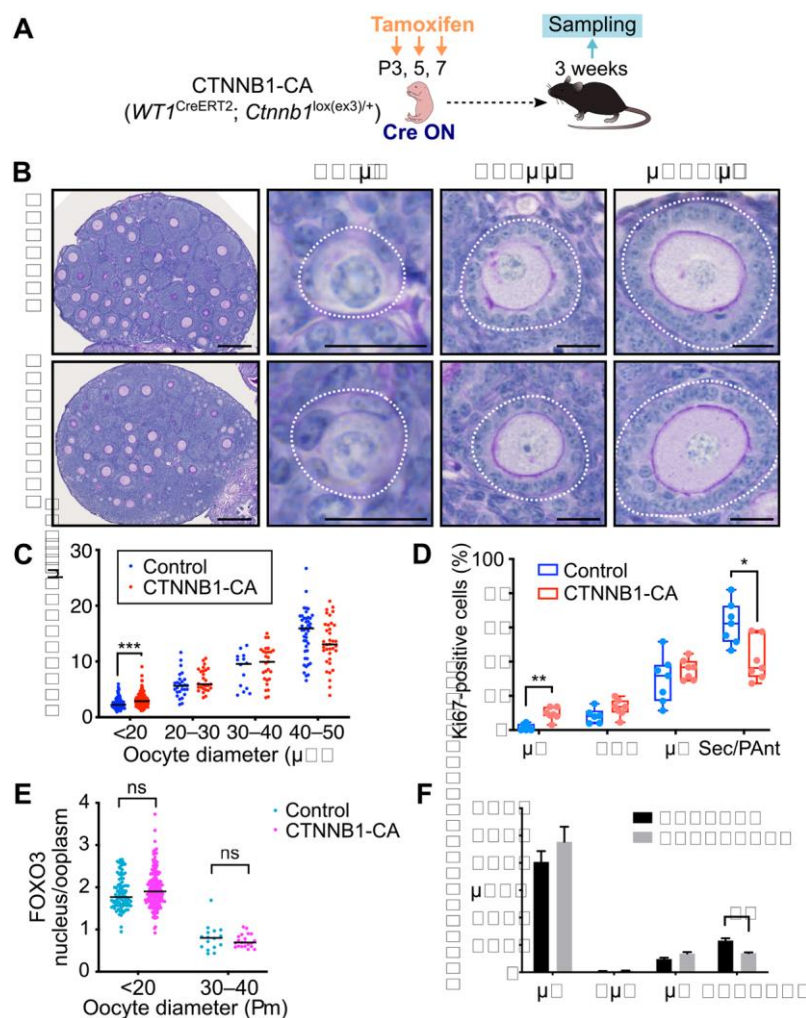


Figure 4. Constitutively active CTNNB1 promotes the pre-GC to GC transition. (A)

Experimental scheme showing induction of a constitutively active form of CTNNB1 in ovarian somatic cells of CTNNB1-CA mice. (B) PAS-H staining of ovarian sections from 3-week-old (tamoxifen-treated) CTNNB1-CA and littermate control mice. Follicles were classified by oocyte size (white dotted lines). Scale bar, 200 μ m (leftmost panels) or 20 μ m (other panels). (C) GC layer thickness categorized by oocyte diameter for 3-week-old CTNNB1-CA and control mice. Horizontal lines represent the median ($n=226$ follicles from five control mice; $n=224$ follicles from five CTNNB1-CA mice). *** $P < 0.001$ (unpaired multiple t tests with the Holm-Sidak correction). (D) Percentage of MKI67-positive pre-GCs/GCs for each follicle type (Int, intermediate) of 3-week-old CTNNB1-CA and control mice as determined by immunofluorescence staining. Boxes indicate the median and 25th and 75th percentiles; whiskers represent minimum and maximum values ($n=7$ mice per genotype). * $P < 0.05$, ** $P < 0.01$

(unpaired multiple t tests with the Holm-Sidak correction). (E) The nucleus/cytoplasm ratio of FOXO3 immunofluorescence intensity for oocytes of 3-week-old CTNNB1-CA and control mice. Horizontal lines represent the median ($n=110$ oocytes from four control mice; $n=216$ oocytes from five CTNNB1-CA mice). ns, not significant (unpaired multiple t tests with the Holm-Sidak correction). (F) Quantification of follicle number per ovary for 3-week-old CTNNB1-CA and control mice. Follicles were classified as primordial (Pm), activated primordial (APF), primary (Pr), or secondary–antral (Sec–Ant). Data are means + s.e.m. ($n=7$ mice per genotype). $**P < 0.01$ (unpaired multiple t tests with the Holm-Sidak correction).

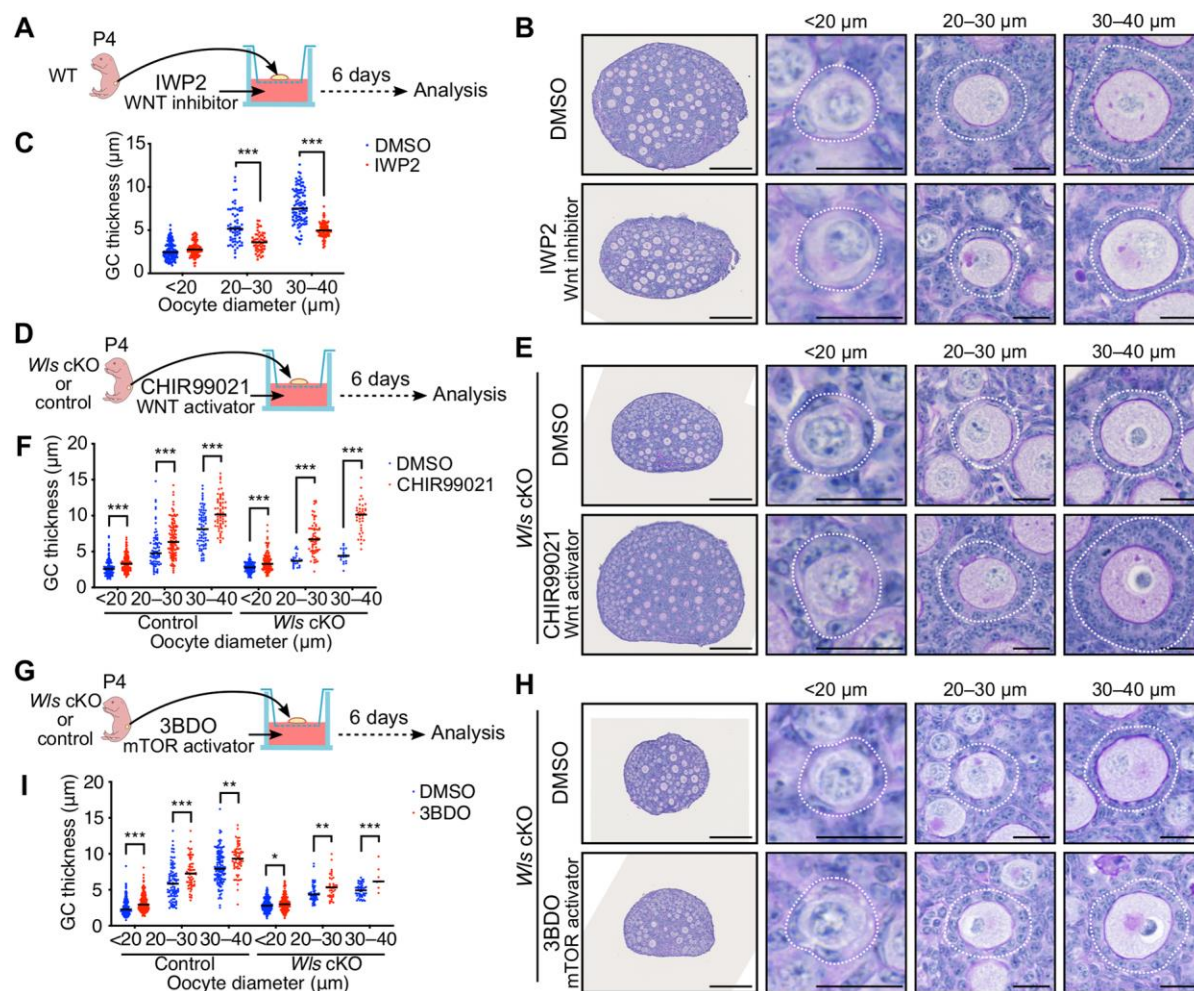


Figure 5. Rescue of the *Wls* cKO ovarian phenotype by a WNT activator in vitro. (A, D, G) Experimental design for culture of ovaries from the indicated mice with the WNT inhibitor IWP2 at 2 μM (A), the WNT activator CHIR99021 at 5 μM (D), or the mTOR signaling activator 3BDO at 100 μM (G) or with the corresponding concentration of DMSO as a vehicle control. (B, E, H) PAS-H staining of sections of ovaries cultured for 6 days with IWP2 (B), CHIR99021 (E), or 3BDO (H). Follicles were classified by oocyte diameter and are demarcated by the white dotted lines. Scale bar, 200 μm (leftmost panels) or 20 μm (other panels). (C, F, I) GC layer thickness categorized by oocyte diameter for ovaries cultured with IWP2 (C), CHIR99021 (F), or 3BDO (I). Horizontal lines represent the median. (DMSO, $n=280$; IWP2, $n=220$ (C). Control +DMSO, $n=245$; control +CHIR99021, $n=348$; *Wls* cKO +DMSO, $n=162$; *Wls* cKO +CHIR99021, $n=223$ (D). Control +DMSO, $n=457$; control +3BDO, $n=330$; *Wls* cKO +DMSO,

$n=360$; Wls cKO +3BDO, $n=274$ (E).) $*P < 0.05$, $**P < 0.01$, $***P < 0.001$ (unpaired multiple t tests with the Holm-Sidak correction).

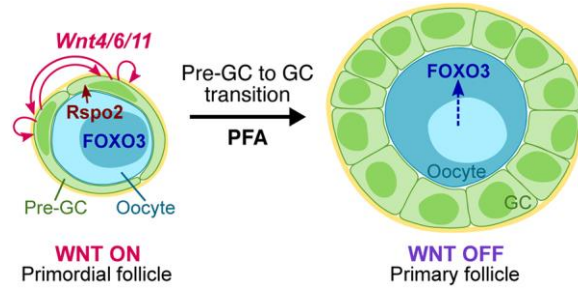


Figure 6. Proposed role of WNT signaling in folliculogenesis. WNT-responding pre-GCs produce *Wnt4*, *Wnt6*, and *Wnt11* in primordial follicles and oocytes secrete the WNT agonist RSPO2. Activation of canonical WNT signaling in pre-GCs promotes their transition into GCs during PFA. In primary follicles, GCs induce the withdrawal of oocytes from a dormant state, as reflected by the translocation of FOXO3 from the nucleus to the cytoplasm.

Supplementary Information

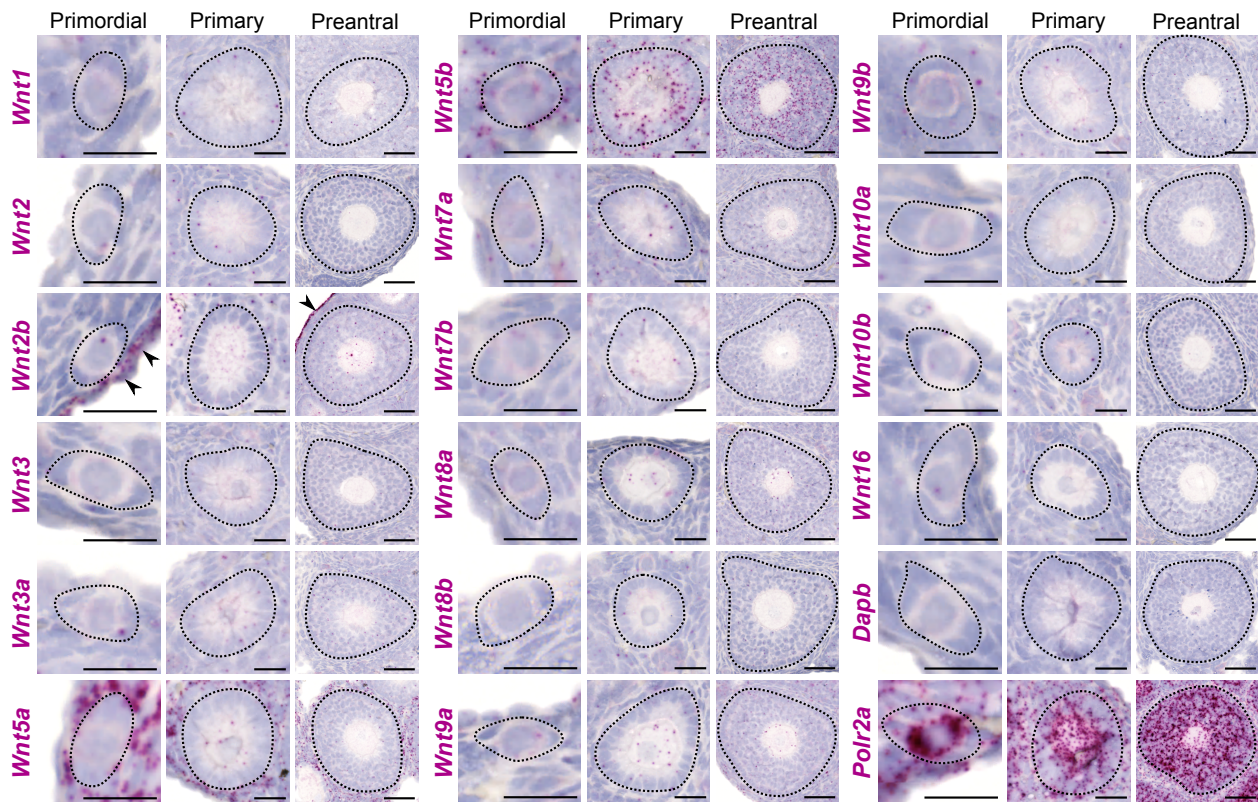


Figure S1. Expression pattern of Wnt ligands in mouse ovary.

In situ hybridization analysis of *Wnt1*, *Wnt2*, *Wnt2b*, *Wnt3*, *Wnt3a*, *Wnt5a*, *Wnt5b*, *Wnt7a*, *Wnt7b*, *Wnt8a*, *Wnt8b*, *Wnt9a*, *Wnt9b*, *Wnt10a*, *Wnt10b*, *Wnt16*, *Dapb* (negative control), and *Polr2a* (positive control) mRNAs (red) in ovaries of 3-week-old WT mice. Follicles were classified as primordial, primary, or preantral (dotted lines). Arrowheads indicate the ovarian epithelium. Scale bar, 50 μ m (rightmost panels) or 20 μ m (other panels).

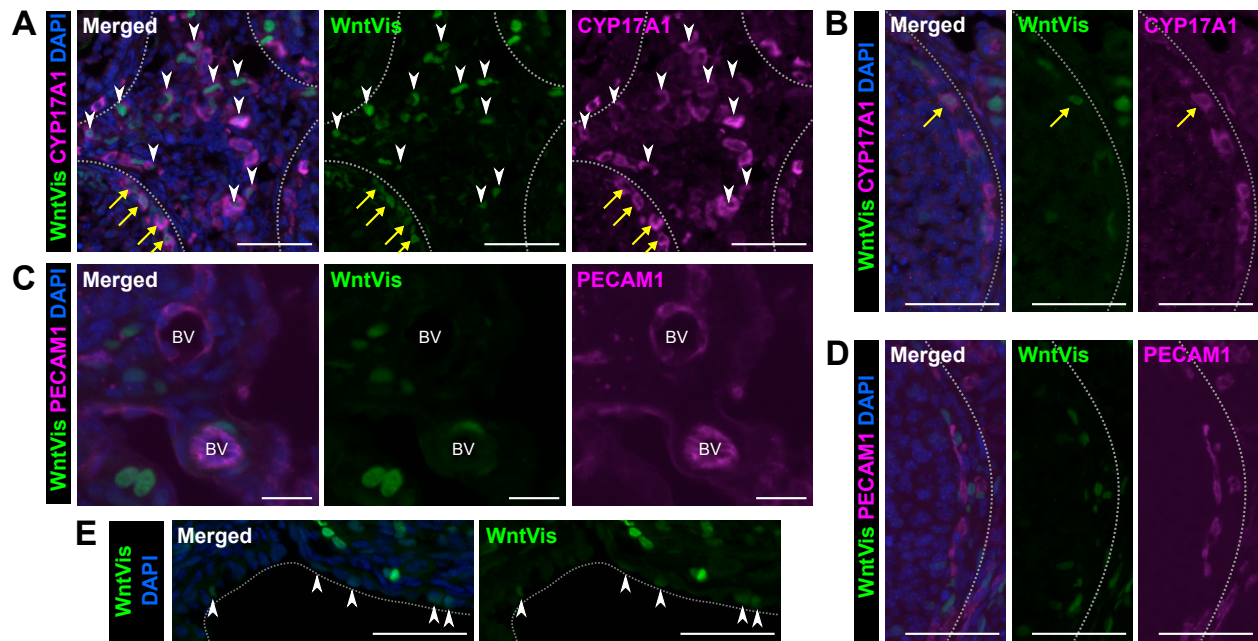


Figure S2. Interstitial cells, Theca cells, and ovarian epithelium receive Wnt signals.

(A, B) Immunofluorescence staining of WntVis (green) and CYP17A1 (magenta) in stromal (A) or Theca cell (B) regions of ovaries from 4-week-old *R26-WntVis* mice. Nuclei were counterstained with DAPI (blue). White arrowheads indicate interstitial cells which are double-positive for WntVis and CYP17A1. Yellow arrows indicate Theca cells which are double-positive for WntVis and CYP17A1. Gray dotted lines mark the boundaries of antral follicles. Scale bar, 50 μ m.

(C, D) Immunofluorescence staining of WntVis (green) and PECAM1 (magenta) in blood vessels (C) or capillary vessels around follicles (D) of ovaries from 4-week-old *R26-WntVis* mice. Nuclei were counterstained with DAPI (blue). Gray dotted lines mark the boundaries of antral follicles. BV, blood vessels. Scale bar, 20 μ m (C) or 50 μ m (D).

(E) Immunofluorescence staining of WntVis (green) in ovarian epithelium of 4-week-old *R26-WntVis* mice. Nuclei were counterstained with DAPI (blue). The gray dotted lines mark the boundaries of ovaries. Scale bar, 50 μ m. Arrowheads indicate WntVis-positive ovarian epithelium.

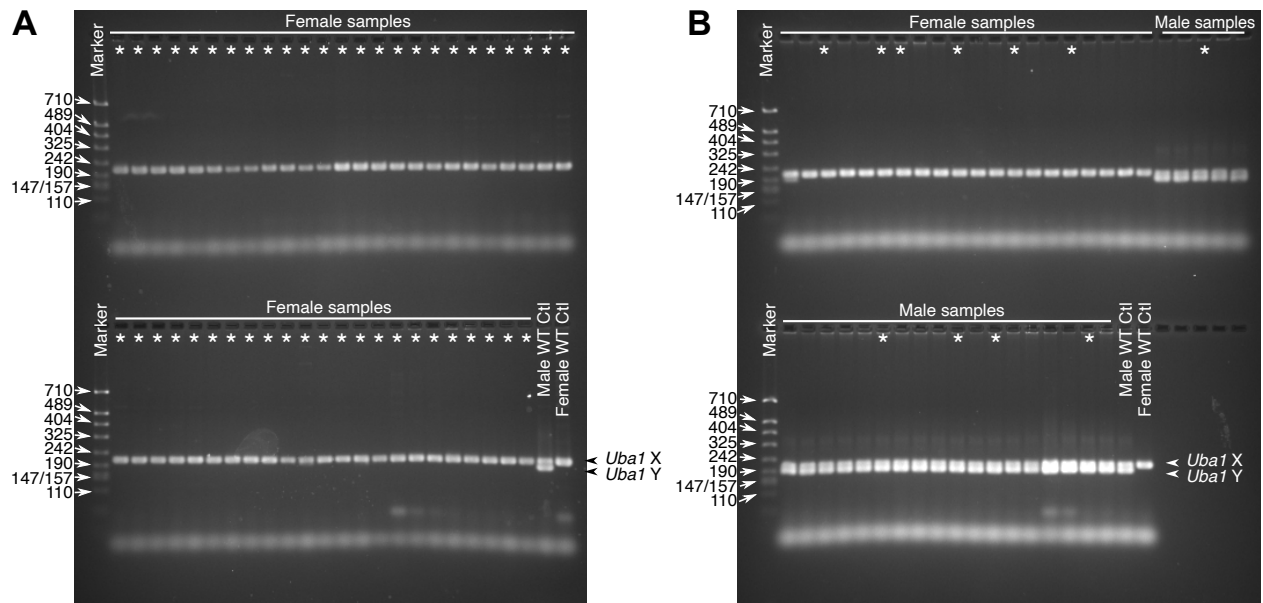


Figure S3. Sex genotyping of *Wls* cKO mice.

(A, B) Sex genotyping was performed on collected female *Wls* cKO mouse samples (A) or female/male mice obtained from a single in vitro fertilization (B). PCR-amplified products using primer sets for *Uba1* gene were analyzed by agarose gel electrophoresis with full images. Female product, single band of 217 bp; male samples, distinct bands of 198 and 217 bp. Each lane represents one independent sample. Asterisks indicate *Wls* cKO mice. Male or female wildtype (WT) mice were used as controls.

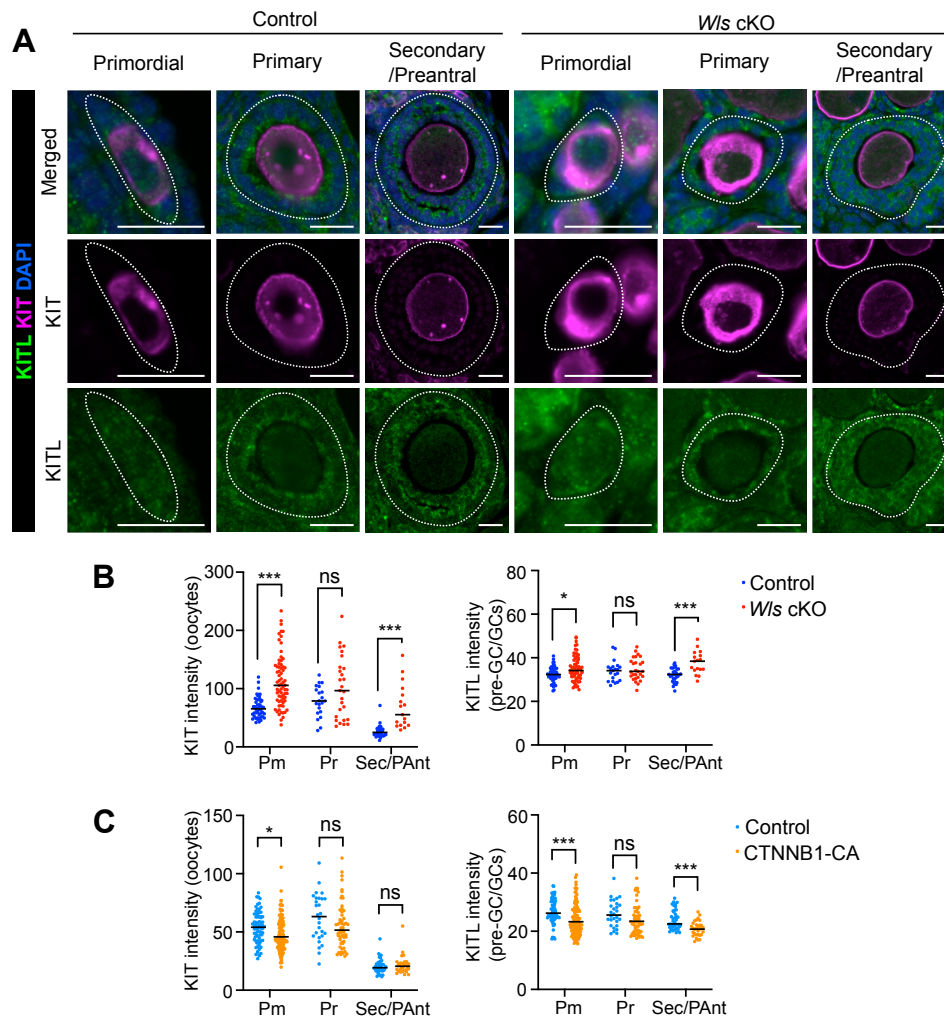


Figure S4. KIT and KITL expression in *Wls* cKO or CTNNB1-CA mice.

(A) Immunofluorescence staining of KITL (green) and KIT (magenta) in the ovaries of 3-week-old *Wls* cKO or littermate control mice. Nuclei were counterstained with DAPI (blue). Follicles are demarcated with white dotted lines. Scale bar, 20 μ m.

(B, C) Fluorescence intensities of KIT in oocytes and KITL in pre-GC/GCs in the ovaries of *Wls* cKO (B), tamoxifen-treated CTNNB1-CA (C) or littermate control mice at 3 weeks of age. Follicles were morphologically classified (Pm, primordial; Pr, primary; Sec/PAnT, secondary/preantral). Horizontal lines represent the median. ns, not significant, * $P < 0.05$, *** $P < 0.001$ (unpaired multiple t tests with Holm-Sidak correction). ($n=110$ follicles from five control mice; $n=113$ follicles from five *Wls* cKO mice (B). $n=146$ follicles from five control mice; $n=203$ follicles from five CTNNB1-CA mice (C).) The intensities from *Wls* cKO (B) and CTNNB1-CA (C) mice are not directly comparable because the data were obtained from different experiments.

	Primary					Secondary/Preantral				
	squamous	s/c	cuboidal	c/c	columnar	squamous	s/c	cuboidal	c/c	columnar
Control	6 (6.6%)	8 (8.8%)	12 (13.2%)	5 (5.5%)	8 (8.8%)	0 (0.0%)	1 (1.1%)	7 (7.7%)	0 (0.0%)	44 (48.4%)
<i>Wls</i> cKO	16 (26.2%)	12 (19.7%)	7 (11.5%)	1 (1.6%)	0 (0.0%)	0 (0.0%)	8 (13.1%)	17 (27.9%)	0 (0.0%)	0 (0.0%)

Table S1. Contingency table showing the phenotypic differences of developing follicles classified by GC morphology in 2-week-old *Wls* cKO (n = 61) and control (n = 91) mice.

	Primary					Secondary/Preantral				
	squamous	s/c	cuboidal	c/c	columnar	squamous	s/c	cuboidal	c/c	columnar
Control	2 (2.4%)	4 (4.9%)	15 (18.3%)	5 (6.1%)	4 (4.9%)	0 (0.0%)	0 (0.0%)	0 (0.0%)	1 (1.2%)	51 (62.2%)
PN- <i>Wls</i> cKO	42 (35.6%)	35 (29.7%)	12 (10.2%)	2 (1.69%)	1 (0.9%)	2 (1.69%)	11 (9.32%)	12 (10.2%)	1 (0.9%)	0 (0.0%)

Table S2. Contingency table showing the phenotypic differences of developing follicles classified by GC morphology in 3-week-old tamoxifen-treated PN-*Wls* cKO (n = 118) and control (n = 82) mice.